Ministry of Higher Education & Scientific Research
Ninevah University
College of Electronics Engineering
Communication Engineering Department

New Method for Improving Image Quality in Ultrafast Ultrasound Imaging

By

Shahad Abdulsalam Thanoon

M.Sc. Dissertation

In

Communication Engineering

Supervised by

Asst. Prof. Dr. Mahmod. A. Al_Zubaidy

Dr. Zainab Rami Alomari

2024 A.D. **1445 A.H.**

Ministry of Higher Education & Scientific Research
Ninevah University
College of Electronics Engineering
Communication Engineering Department

New Method for Improving Image Quality in Ultrafast Ultrasound Imaging

A Dissertation Submitted by

Shahad Abdulsalam Thanoon

To

The Council of College of Electronic Engineering

University of Ninevah

In Partial Fulfillment of the Requirements

For the Degree of Master of Sciences

In

Communication Engineering

Supervised by

Asst. Prof. Dr. Mahmod. A. Al_Zubaidy

Dr. Zainab Rami Alomari

2024 A.C. **1445A**

بِسْمِ اللَّـهِ الرَّحْمَـٰنِ الرَّحِيمِ

((رَبِّ أَوْزِعْنِي أَنْ أَشْكُرَ نِعْمَتَكَ الَّتِي أَنْعَمْتَ عَلَيَّ وَعَلَىٰ وَالِدَيَّ وَأَنْ أَعْمَلَ صَالِحًا تَرْضَاهُ وَأَدْخِلْنِي بِرَحْمَتِكَ فِي عِبَادِكَ الصَّالِحِينَ))

صدق الله العظيم

سورة النمل الآية (19)

Supervisor's Certification

We certify that the dissertation entitled (**New Method for Improving Image Quality in Ultrafast Ultrasound Imaging**) was prepared by **Shahad Abdulsalam Thanoon** under our supervision at the Department of Communication Engineering, Ninevah University, as a partial requirement for the Master of Science Degree in Communication Engineering.

Signature:

Name: Assist. Prof. Dr. Mahmod. A. Al_Zubaidy

Date: 19 /3/2024

Signature: Z. R. S

Name: Dr. Zainab Rami Alomari

Date: 19 /3/2024

Report of Linguistic Reviewer

I certify that the linguistic reviewing of this dissertation was carried out by me and it is accepted linguistically and in expression.

Signature: Essam

Name: Essam Tahir Muhammed

Date: / 3/2024

Report of the Head of Department

I certify that this dissertation was carried out in the Department of Communication Engineering. I nominate it to be forwarded to discussion.

Signature:

Name: Assist. Prof. Dr. Mahmod. A. Al_Zubaidy

Date: 19 /3 /2024

Report of the Head of Postgraduate Studies Committee

According to the recommendations presented by the supervisors of this dissertation and the linguistic reviewer, I nominate this dissertation to be forwarded to discussion.

Signature:

Name: Assist. Prof. Dr. Mahmod. A. Al_Zubaidy

Date: 19 / 3/2024

Committee Certification

We the examining committee, certify that we have read this dissertation entitled (**New Method for Improving Image Quality in Ultrafast Ultrasound Imaging**) and have examined the postgraduate student (**Shahad Abdulsalam Thanoon**) in its contents and that in our opinion; it meets the standards of a dissertation for the degree of Master of Science in Communication Engineering.

Signature:

Name: Assist. Prof. Dr. Younis Mahmood Abbosh
Head of committee
Date: / 3/2024

Signature:

Name: Assist. Prof. Dr. Basma MohammedKamal Younis
Member
Date: / 3 /2024

Signature:

Name: Assist. Prof Dr.Safwan Hafeedh Younus
Member
Date: 19/ 3 /2024

Signature:

Name: Assist. Prof. Dr. Mahmod. A. Al_Zubaidy
Member and Supervisor
Date: 19 / 3 /2024

Signature: Z.R.Sal

Name: Dr. Zainab Rami Alomari
Member and Supervisor
Date: 19 / 3 /2024

The college council, in its .... meeting on / / 2024 , has decided to award the degree of Master of Science in Communication Engineering to the candidate.

Signature:

Name: Prof. Khaled Khalil Muhammad

Dean of the College

Date: / /2024

Signature:

Name: Assist. Prof. Dr. Bilal A. jebur

Council registrar

Date: / /2024

ACKNOWLEDGEMENTS

At the outset, I thank God Almighty for all the blessings He bestowed upon me in my life. Words cannot express my gratitude to my supervisors for their invaluable patience and feedback. I also could not have undertaken this journey without them, who generously provided knowledge and expertise. Additionally, this endeavor would not have been possible without my family, especially my parents, my husband, and my children, my brothers and sister, their belief in me has kept my spirits and motivation high during this process. Lastly, I am thankful to God Almighty, and I dedicate this dissertation to my parents and to everyone who helped me during my academic career.

Researcher

Shahad Abdulsalam

2024

ABSTRACT

Medical imaging is a modern tool used in diagnosing diseases and injuries, including tumors and cancers. Various types, including CT, X-ray, MRI, and ultrasound, are used. Ultrasound imaging is popular due to its non-invasive, cost-effectiveness, high tumor identification ability, and lack of anesthesia, offering high frame rates but sacrificing image quality. The type of ultrasound imaging that uses no focusing is called Plane-Wave Imaging (PWI). Researchers and engineers are enhancing imaging quality through various techniques, including adaptive beamforming technologies, with Minimum Variance (MV) adaptive beamformer improving resolution and Eigen Space-Based Minimum Variance (ESBMV) adaptive beamformer enhancing contrast. However, ESBMV has a drawback of producing black box regions (BBR) and dark spots in the produced images. Partial-ESBMV (PESBMV) method has been recently proposed to control those artifacts with a slight reduction in contrast. In this dissertation, a beamforming method is proposed to improve the imaging quality of PESBMV. This approach uses two factors as detection tools to adaptively indicate the different regions of the image. Those factors are the number of vectors in the signal subspace matrix produced by ESBMV and the weight of ESBMV. After discrimination, which divides the image into four regions, the most suitable beamforming method is applied in each of those regions. The results of applying the proposed method, MV, ESBMV, and PESBMV to in vitro datasets and simulation data using MATLAB (R2021a) show the superiority of the proposed method in improving speckle preservation with (55%) resolution improvement, compared to PESBMV, in addition to providing excellent contrast compared to the other implemented methods.

TABLE OF CONTENTS

LIST OF FIGURES

LIST OF TABLES

LIST OF ABBREVIATIONS

Abbreviation	Name
2D	Two Dimension
3D	Three Dimension
4D	Four Dimension
BBR	Black Box Region
BTI	Backscatter Tensor Imaging
CF	Coherence Factor
CNN	Convolutional Neural Network
CNR	Contrast To Noise Ratio
CPWI	Compound Planewave Imaging
CR	Contrast Ratio
CT	Computed Tomography
CUDA	Coronary Ultrafast Doppler Angiography
DAS	Delay And Sum
dB	Decibel
DMAS	Delay Multiple And Sum
DNN	Deep Neural Network
ESBMV	Eigen Space Based Minimum Variance
ETI	Elastic Tensor Imaging
FWHM	Full Width at Half Maximum
LV	Left Ventricle
MRI	Magnetic Resonance Imaging
MS	Myocardial Stiffness
MV	Minimum Variance

NDT	Non-Destructive Testing
OCT	Optical Coherent Tomography
PCI	Phase Coherence Imaging
PESBMV	Partial Eigen Space Based Minimum Variance
PSF	Point Spread Function
PWI	Plane Wave Imaging
SA	Synthetic Aperture
SCF	Sign Coherence Factor
SLSC	short-lag spatial coherence
SNR	Signal-To-Noise Ratio
SSNR	Speckle Signal-To-Noise Ratio

LIST OF SYMBOLS

Symbol	Name
$\boldsymbol{\lambda_i}$	The $i\ th$ eigenvalue of the covariance matrix
$\boldsymbol{CM}$	Covariance matrix
$\boldsymbol{U_n}$	Noise subspace matrix
$\boldsymbol{U_s}$	Signal subspace matrix
$\boldsymbol{L_p}$	Subarray length in spatial smoothing operation
$\boldsymbol{Num}$	The number of columns in the signal subspace matrix
$\boldsymbol{T_j}$	The value received by the $j\ th$ element
$\boldsymbol{T_s}$	Time sampling
$\boldsymbol{T_{si}}$	The time between the transmit and receive for a scan line
$\boldsymbol{V_p}$	The $p\ th$ subarray
$\boldsymbol{W_{ESBMV}}$	The weighting vector of ESBMV
$\boldsymbol{W_{PESBMV}}$	The weighting vector of PESBMV
$\boldsymbol{Y_{CF}}$	Coherence Factor-weighted output
$\boldsymbol{a}$	the steering vector
$\boldsymbol{f_S}$	Sampling frequency
$\boldsymbol{f_0}$	Central frequency
$\boldsymbol{r_i}$	Distance from the point to element i
$\boldsymbol{t_i}$	the delay needed to be applied to the i^{th} element data
$\boldsymbol{v_i}$	is the i^{th} orthonormal eigenvector for λ_i
$\wedge$	Diagonal matrix whose diagonal is the eigenvalues of the covariance matrix
$\boldsymbol{PRF}$	Frame rate

$\boldsymbol{K}$	Temporal averaging coefficient
$\boldsymbol{M}$	The total number of elements in the transduce
$\boldsymbol{P}$	The number of subarrays
$\boldsymbol{U}$	A matrix contains the eigenvectors of the covariance matrix
$\boldsymbol{Y}$	Beamformer output
$\boldsymbol{c}$	Sound speed
$\boldsymbol{k}$	The wave number
$\boldsymbol{p}(\boldsymbol{x},\mathbf{y},\boldsymbol{z})$	The value of the point located at $(\boldsymbol{x},\mathbf{y},\boldsymbol{z})$in the image
$\boldsymbol{w}$	The weighting vector
$\boldsymbol{x}$	Lateral distance
$\boldsymbol{\delta}$	ESBMV coefficient
$\boldsymbol{\eta}$	PESBMV coefficient
$\boldsymbol{\mu}$	Mean value
$\boldsymbol{\sigma}$	Standard deviation

CHAPTER ONE

INTRODUCTION

1.1 Introduction

Medical imaging is a non-invasive technology that acquires signals by leveraging the physical principles of sound, light, electromagnetic waves, etc., from which visual images of internal tissues of the human body are generated. Medical imaging is a vital component of modern healthcare, playing a role in the diagnosis, staging, and monitoring of many diseases and conditions. There are many widely used medical imaging modalities, including ultrasound, digital radiography, computed tomography (CT), magnetic resonance imaging (MRI), and optical coherent tomography (OCT) [1].

Recurrent imaging is used for managing various health conditions and chronic diseases such as malignancies, trauma, end-stage kidney disease, cardiovascular diseases, Crohn's disease, urolithiasis, and cystic pulmonary disease. However, recurrent radiological imaging and associated cumulative doses to patients can lead to radiation exposure and cancer risk elevation. Therefore, it is important to improve radiation protection of individuals who are submitted to frequent imaging. This includes access to dose-saving imaging technologies, improved imaging strategies and appropriateness process, specific optimization tailored to the clinical condition and patient habitus, wider utilization of the automatic exposure monitoring systems with an integrated option for individual exposure tracking in standardized patient-specific risk metrics, improved training, and communication. Non-ionizing imaging structures like ultrasound can be used to prevent exposure to radiation [2].

Using ultrasound imaging is advantageous over other imaging methods. It is a better option than other imaging procedures like MRI, X-rays, and CT because of its non-invasive nature.

Ultrasound imaging gives real-time body structure images, non-ionizing radiation exposure, high tumor detection, no anesthetic required, and may break up urinary stones, making it a safe and cost-effective procedure.

Contrast chemicals are used in several imaging methods, such as CT and MRI scans, to boost visibility of specific tissues or organs. The risk of adverse reactions to contrast agents is lowered since ultrasonic imaging does not need the use of these agents.

Because ultrasound devices are portable and generally affordable in comparison to other imaging equipment, they are more accessible to healthcare professionals in distant or low-resource areas.

Ultrasound imaging uses high-frequency sound waves that are higher than the audible frequency to generate images of inside tissues and organs.[3], [4]. It is one of the most rapidly evolving medical imaging techniques. It is used as a popular diagnostic tool in a variety of applications, including cardiac imaging, abdominal, fetal, and breast imaging. Real-time images are used to provide rapid visual guidance for a variety of interventional procedures, such as regional anesthesia and pain control. Figure 1.1 shows the components of sonography.

Figure (1.1): Sonography components [5].

Acoustic waves with frequencies ranging from 20 kHz to 20 MHz represent ultrasound signals. Electrical stimulation of a piezoelectric transducer results in the generation and detection of those waves. Ultrasound transducers are used to transmit and receive ultrasound waves. The transducer is the most essential equipment in ultrasonic imaging, which differs according to the number and arrangement of the piezoelectric element’s arrays, which shapes the way it is used and the application where it is employed [6].

The Curie brothers demonstrated the piezoelectric effect by mechanically stressing a cut piece of quartz [3], [4]. They subsequently discovered the reverse piezoelectric effect, which occurs when an electrical current is applied to quartz and causes quartz vibrations [3], [7]. When these mechanical sound waves pass through body tissues, they create alternating areas of compression and rarefaction. A piezoelectric effect is a phenomenon where certain materials generate an electric charge in response to applied mechanical stress. This effect is beneficial for various applications, such as photocatalysis, superconductivity and sensing.

A piezoelectric effect creates sound waves and propagation requires a transmission medium [6]. Ultrasound waves are sent to deeper layers, reflect back to the transducer as echoes, scatter, and transform into heat while passing through tissues. The velocity of propagation differs according to the characteristics of the medium, and the images result from the interaction of refraction, reflection, scattering, absorption, attenuation, and transmission [6], [8]. Figure (1.2) shows the two phases of transmission and reception of ultrasound signals using a linear array transducer.

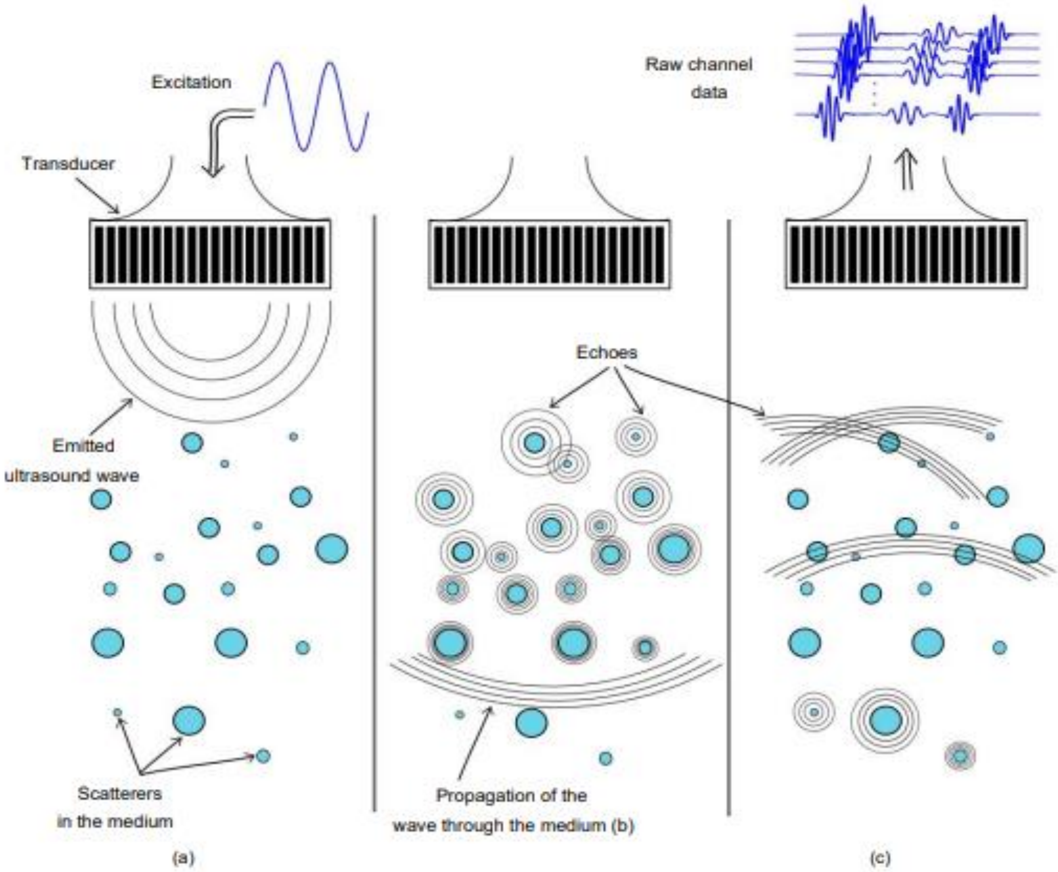

Figure (1.2) :(a) The transducer emitted ultrasound wave into medium. (b) the transducer converts the reflected waves into electrical signals [9].

When Ultrasound waves travel through tissues and partly being transmitted to deeper structures, echoes are partially being reflected back to the transducer, scattered, and converted to heat. In ultrasound imaging, the return of echoes to the transducer for imaging purposes is of prime importance.

Acoustic impedance is a tissue parameter that determines how much echo is returned after a tissue interface is contacted. This is a physical property of a medium defined as the density of the medium multiplied by the velocity of ultrasound wave propagation in the medium. Air-containing organs (such as the lung) have the lowest acoustic impedance, whereas dense organs like bone have extremely high acoustic impedance [3]. The intensity of the reflected echo is proportional to the difference (or mismatch) in acoustic impedances between two mediums. No echo is produced if the acoustic impedance of two tissues is the same. Low-intensity echoes are commonly produced at the interfaces of soft tissues with similar acoustic impedances. Because of the large acoustic impedance gradient, interfaces between soft tissue and bone or the lung produce very intense echoes [3].

Ultrafast ultrasound imaging is a technique that allows the analysis of rapidly changing physical phenomena in human body, such as ultrasensitive flow imaging in the cardiovascular system or shear-wave elastography.

Ultrafast ultrasound, an acquisition technique that has been widely studied and applied over the last two decades, As the name implies, ultrafast ultrasound imaging can potentially exceed 1,000 frames per second by overcoming the conventional frame rate limitation which is usually much less than 1000 frames per second [10]. By delaying pulse times across a group of transducer elements, in transmission, conventional ultrasonography emphasizes the shape and steering of focused acoustic beams. To scan a 2D or 3D space, focused beams are transmitted and received line by line. This simple scheme, however, limits the frame rate to about 100 frames per second, which only meets the basic requirements of traditional medical applications.

1.2 Literature Review

Ultrasound has been used for imaging human body for over 50 years. Dr. Karl Theo Dussik, an Austrian neurologist, pioneered the use of ultrasound as a medical diagnostic tool to view the brain [3]. In medicine, ultrasound has become one of the most widely used imaging modalities. Underwater acoustics, monitoring and control applications, medical ultrasonics for therapy, diagnosis, and surgery, biotechnology, nanotechnology, and defense are all diverse disciplines of research within ultrasonics.

To generate high-quality images using PWI and overcome unfocused transmission drawbacks, resembled by the decreased image quality, in terms of both contrast and resolution, various techniques have been proposed in recent decades.

Those methods include the adaptive and non-adaptive beamforming techniques. In the medical field, adaptive beamforming methods can increase image quality while degrading real-time performance, due to requiring long processing time. Researchers have devised an adaptive beamforming method based on minimum variance and Deep Neural Network (DNN) to increase image efficiency and speed up the beamforming process in ultrafast ultrasound [11].

The Eigenspace-Based Minimum Variance Beamformer (ESBMV) is an adaptive beamforming technique used in medical ultrasound imaging. It is used to suppress sidelobes, grating lobes and clutter for PWI, and it can improve image quality by reducing speckle pattern inconsistencies and removing artifacts. This method is utilized in ultrasonic imaging in medicine to improve the resolution and contrast of images [12], [13].

ESBMV was first introduced by Van Veen in (1988) [14]. It was developed to highly improve the contrast of MV beamformer. However, it may introduce dark region artifacts alongside the hyperechoic scatterers when obtaining obvious contrast. A dark region produced artificially in ESBMV is called Black Box Region (BBR). In addition to BBR, ESBMV produces dark regions in background speckle, distorting its homogeneity.

Lately, several research groups have investigated and developed several ways to improve ESBMV beamforming.

In (2010), Mahloojifar and Asl, employing a simulated cyst phantom, proposed using iterative ESBMV to determine appropriate imaging parameter choices to improve imaging quality. Nonetheless, the impact of changed parameters on BBR artifacts was not taken into account in the proposed iterative approach [15].

In (2012), Zeng *et al*. proposed mixing ESBMV with Wiener post-filtering to increase ESBMV contrast and resolution.[16]. However, the suggested combination failed to eliminate the BBR artifacts and black spots in the background speckle.

In (2013), Zeng *et al.* suggested a beam-domain ESBMV beamformer by combining the beam-space approach with the ESBMV beamformer. The suggested approach can achieve performance equivalent to that of the ESBMV beamformer in considerably less time, however ESBMV artifacts still exist.[17] .

In (2015), Aliabadi *et al.* suggested a technique that able to reduce dark spot and enhance contrast in ESBMV through adjusting the focal point value with respect to the characteristics of the echo signals received by the surrounding locations [18]. However, this proposed technique failed to be removing BBR artifacts.

In (2016), Zhao *et al.* suggested a technique that able to advances image quality in clear of speckle homogeneity, contrast, and resolution [19], though associations ESBMV with a subarray-based coherence factor. However, this approach failed to be removing BBR artifacts and Subarray smoothing has a negative impact on computation efficiency.

In (2017), Partial-ESBMV (PESBMV) method was suggested to overcome the ESBMV limitation and its artifacts. This approach applies or stops ESBMV based on the number of eigenvectors in the signal subspace. As a result, this strategy was able to decrease BBR artifacts [20]. However, the contrast in PESBMV is lower in comparison to reference ESBMV. Following that, several techniques for improving ESBMV's performance were proposed.

In (2017), Wu *et al.* proposed an adjustable factor to adaptively assign some special imaging parameters, and then combined ESBMV beamformer with it, to improve the spatio-temporally smoothed factor beamformer by introducing. However, BBR artifacts were not eliminated [21].

In (2017), Wang *et al.* suggested a synthetic aperture (SA) ultrasound imaging technique combining short-lag spatial coherence (SLSC) weighting with ESBMV, to improve imaging quality at all depths. Based on the spatial coherence of different sources, an adaptive threshold of eigenvalues is designed for ESBMV. As a result, this strategy was able to increase contrast while the contrast to noise ratio and speckle SNR are decreased due to the presence of BBRs [22].

In (2017), Mozaffarzadeh *et al.* suggested linking ESBMV with Delay Multiply And Sum (DMAS) beamformer to reduce sidelobes and raise the signal-to-noise ratio through a simulated study. However, this did not reduce the ESBMV artifacts [23].

In (2019), Mozaffarzadeh *et al.* suggested again to link ESBMV with DMAS beamformer to reduce sidelobes and raise the signal-to-noise ratio for the application of Linear-Array Photoacoustic Imaging. This method raised the signal-to-noise ratio and increased resolution but BBR and dark spot were sill exist [24].

In (2020), Shamekhi *et al*. proposed to combine ESBMV beamformer with the Sign Coherence Factor (SCF) to reduce noise when they are used in combination with each other [25]. But artifacts of ESBMV still occur.

In (2021), Lan *et al.* suggested the use of an adaptive eigenvalue threshold for subspace development to improve contrast and reduce dark region artifacts [26]. Image quality can be improved by adaptively altering the subarray length of the covariance matrix, this also helps to decrease the size of the covariance matrix and, to some extent, increase computational efficiency. However, this suggestion produced a lower hyperechoic target brightness compared to classical ESBMV, and according to that the borders of hyperechoic targets were suffering from a lack of clarity.

Table 1-1: Literature reviews.

Year of Study	**No of Reference**	**Study Description**	**Advantages**	**Disadvantage**
1988	[14]	It was developed to highly improve the contrast of MV beamformer	Avoidance of explicit covariance matrix estimation and inversion, requiring only scalar and vector quantities to be estimated	ESBMV artifacts
2010	[15]	ESBMV beamforming has been successfully applied to specific ultrasound techniques, such as	improved imaging resolution and contrast, better performance, and application to specific ultrasound	BBR artifacts

		plane wave imaging in ultrasound computed tomography, where it has been shown to maintain or improve the resolution and contrast ratio of the reconstruction results	techniques.	
2012	[16]	It has been combined with Wiener postfilter to further improve medical ultrasound imaging quality	optimizes the ESBMV weights with a Wiener postfilter, making the output power of the new beamformer closer to the actual signal power at the imaging point than the ESBMV beamformer	failed to eliminate the BBR artifacts and black spots in the background speckle
2013	[17]	It combines the beamspace method with the Eigenspace-Based Minimum Variance (ESBMV)	The proposed method can achieve performance comparable to the ESBMV beamformer within	ESBMV artifacts still exist.

		beamformer	much shorter time	
2015	[18]	The proposed beamforming method utilizes a kernel to select neighbor points, and the number of selected eigenvectors for each focal point is compared with the number of selected eigenvectors of its neighbor points and is changed to a new value	This method enhances the imaging contrast significantly while keeping the resolution quality similar to the eigenspace-based minimum variance (ESBMV) beamformer	failed to be removing BBR artifacts.
2016	[19]	This method introducing an adjustable factor to adaptively assign some special imaging parameters and then combining the eigen space-based minimum variance beamformer into the method to	The proposed method improves the robustness of the algorithm with speckle pattern consistency and markedly removes the artifacts while preserving effective ability to suppress clutter and side-lobes	failed to be removing BBR artifacts and Subarray smoothing has a negative impact on computation efficiency

		further improve the image quality.		
2017	[20]	this method, ESBMV is applied or stopped based on the amount of eigenvectors in the signal subspace	this strategy was able to decrease BBR artifacts	the contrast in PESBMV is lower in comparison to reference ESBMV.
2017	[21]	proposed an adjustable factor to adaptively assign some special imaging parameters, and then combine ESBMV beamformer into our method, to improve the spatio-temporally smoothed factor beamformer by introducing.	enhance image contrast and suppress clutter in ultrasound imaging	BBR artifacts were not eliminated
2017	[22]	suggested a synthetic aperture (SA) ultrasound imaging technique combining short-lag	improve imaging quality at all depths, increase contrast	BBR artifacts were not eliminated

		spatial coherence (SLSC) weighting with ESBMV		
2017	[23]	link ESBMV with Delay Multiply And Sum (DMAS) beamformer	reduce sidelobes and raise the signal-to-noise ratio through a simulated study	did not reduce the ESBMV artifacts
2019	[24]	This study link ESBMV with DMAS beamformer for the application of Linear-Array Photoacoustic Imaging.	This method raised the signal-to-noise ratio and increased resolution	BBR and dark spot were sill exist
2020	[25]	combine ESBMV beamformer with the Sign Factor (SCF) Coherence	reduce noise when they are used in combination with each other	But artifacts of ESBMV still occur
2021	[26]	suggested the use of an adaptive eigenvalue threshold for subspace development to improve contrast and reduce dark region artifacts	Image quality improved by adaptively altering the subarray length of the covariance matrix, increase computational efficiency	produced a lower hyperechoic target brightness compared to classical ESBMV, and according to that the borders

				of hyperechoic targets were suffering from a lack of clarity

1.3 The Aims

The main objective of this dissertation aims to:

1. study the different types of adaptive beamformers used in ultrafast ultrasound imaging.
2. suggest a method for improving imaging quality in these types of beamformers, specifically in ESBMV.
3. Discriminate hyperechoic targets, hypoechoic targets, speckle backgrounds and Black Box Regions from each other.
4. Discrimination helps to use the most suitable beamforming method in each region, resulting in improved overall resolution and contrast of the produced images, with preserved homogeneity at background tissue. The operation includes studying various methods and factors and implementing and applying them to the used in-vitro data, in order to find the amount of difference factor’s value in the image regions. This is followed by testing various types of beamformers in order to select the most appropriate type of each imaging region, leading to an improvement in the overall image quality.

1.4 Dissertation Organization

This dissertation is organized as follows:

The introduction, and literature review presented in chapter one.

In chapter two, the theory and principle of ultrasound imaging, theory of beamforming and adaptive beamforming types, and applications of ultrafast ultrasound imaging are introduced in detail.

In chapter three, the model of the proposed method and the flowcharts that are used to calculate the parameters using this method are given, with the beamforming method used in each imaging region. Chapter four states the results and discussions of applying the proposed method to in vitro datasets. Finally, chapter five provides conclusions as well as future related works.

CHAPTER TWO

THEORY AND PRINCIPLE OF ULTRASOUND IMAGING AND BEAMFORMING TECHNIQUES

2.1 Introduction

This chapter presents an overview of ultrasound imaging and its principle, wavelength, frequency, applications, transducer types, imaging techniques in ultrasound, and beamforming principle. It demonstrates the background method behind the standard data-independent and adaptive beamformers and their main issues. Finally, this chapter describes the methods suggested in the literature to improve the image quality produced by the adaptive beamformer.

2.2 Principle of ultrasound imaging

Ultrasound imaging can be carried out by using various imaging techniques. The main types of these techniques are linear scan, plane-wave emission and synthetic aperture. The technique used in this work is the plane-wave type of emission, or Plane-Wave Imaging (PWI).

Linear array transducers were invented, which consist of a series of elements arranged in straight rows, allowing the generation of different sets of directed and/or concentrated emitted beams [27], [28]. And this can be achieved by manipulating the pulse operation of these parts with specified timing patterns, this can be efficiently achieved.

A single unfocused beam is used by PWI for displaying the imaging region, resulting in a high frame rate of several thousand frames per second. PWI can give a frame rate that is independent on the number of data lines produced for the required imaging width [29]. At each transmit event, an ultrasound wave is transmitted from the whole array aperture by pulsing all the elements in the same time. The emitted sound wave will thus produce a plane wave, which propagates with no focusing. Backscattered echoes are then recorded using all elements on the receive aperture. After the received data is ready, the beamforming operation that produces final B-mode images will take place.

In beamforming operation, the output of the sensor array is processed in order to produce an image that has meaning. The purpose of using sensor array is to enhance the signal-to-noise ratio compared to a single sensor, which is a collection of sensors located at fixed spatial positions. Each element of this array receives data that participate in producing the final image from the received ultrasound echo signals [20]. This process is the most crucial step in revealing the necessary information carried by the reflected echo signals [20].

One of the first major steps in any beamformer is focusing. Delays are employed in transmission to manage the contributions from all transducer elements and hit a specific point, which is referred to as the focal point of emission. Echoes received by elements in reception are delayed to accumulate contributions from the same point in the medium (focal point). Focusing performed using received data during beamforming is called (dynamic focusing). In PWI, transmit focusing is not applied.

2.3 Ultrasound Wavelength and Frequency

The frequencies of ultrasound waves are higher than the limit of audible human hearing, which is 20 kHz, as shown in figure 2.1. Sound waves with frequencies ranging from 1 to 20 MHz are used by medical ultrasonography devices.

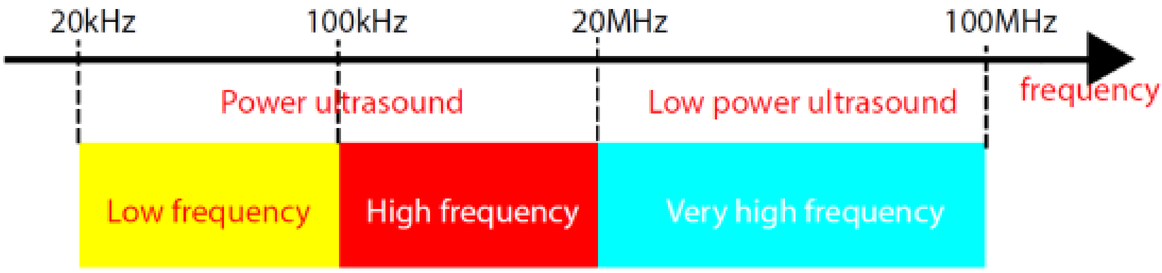

Figure (2.1): Shows the range of ultrasound frequency [30].

The correct transducer frequency selection is critical for achieving optimal image resolution in diagnostic and procedural ultrasound imaging. Ultrasound waves with high spatial resolution are produced by high-frequency (short wavelength) ultrasound waves [3]. This is due to the fact that increasing the amount of compression and rarefaction waves over a given distance allows for more accurate discrimination of two distinct structures along the wave propagation plane. However, because high-frequency waves are more attenuated over a given distance than lower-frequency waves, they are best suited for imaging superficial structures. Low-frequency (long wavelength) waves have lower resolution but can penetrate deeper due to lower attenuation [3]. As a result, in medical ultrasound imaging, high-frequency transducers (up to 10-15 MHz range) are used for imaging superficial structures such as stellate ganglion blocks, and low-frequency transducers (usually 2-5 MHz) are used for imaging deeper tissues such as deep lumbar neuraxial structures.

Ultrasound imaging waves are generated in the form of pulses (intermittent trains of pressure), which usually consist of two or three sound cycles of the same frequency. The pulse repetition frequency (PRF) is the number of pulses emitted by the transducer per unit of time. Before the next pulse is formed, ultrasound waves must be delivered in pulses with enough time between them to allow the signal to reach the target of interest and be reflected back to the transducer as echo. PRF in medical imaging is also known as (frame rate) [3].

2.4 Types of Ultrasound Imaging Transducers

The variety of transducer configurations designed for various applications reflects ultrasound imaging's high flexibility [31]. The widely used types of ultrasound transducers include linear array transducers, phased array transducers and curved array transducers. These types differ in their element organizing, and they are primarily designed for non-invasive use [9], in addition to the presence of other special types of probes that can acquire images invasively. Other types of noninvasive imaging probes include single-element probes, mechanical-2D probes, and 2D-matrix probes, which can acquire acoustical signals from 1D to 3D spaces, respectively [31]

2.5 B-Mode Ultrasound Images

B-mode was initially given this name for distinguishing it from the so-called Amplitude mode (A-mode). In A-mode ultrasound, it is possible to view the amplitude of the signal that is received in a single beam (axial direction) produced by a transducer. When altering to B-mode, along with a transducer's element array (lateral direction), a series of evenly spaced A-mode beams are obtained. In contrast to the beam focusing from a single large element in A-mode, the beam in B-mode is primarily shaped by transmitting ultrasound pulses from an aperture containing a series of smaller elements. B-mode images are the most widely produced image type from medical ultrasound. B-mode image is a two-dimensional image of the scanned area [32], figure 2.2 shows an example B-mode ultrasound Image. Other imaging modes include Doppler flow images, expanded field of view images, and three-dimensional images [6], [32]. The axial direction in a B-mode image is the direction of ultrasonic propagation along the beam line, while the lateral direction is the direction in the image plane perpendicular to the axial direction, parallel to the transducer surface.

The significant proportion of ultrasound transducers is used to generate 2D images. Volumetric B-mode images can be created by stacking 2D planes obtained by mechanical translation along the plane orthogonal to the axial-lateral plane, known as the Elevation direction, by rotating the probe, or by extending the 1D element array transducers to 3D. The quality of B-mode image can be enhanced by improving focusing, producing denser-spaced lines, compounding multiple frequencies, focal depths, and steering angles. Signal processing and image processing methods are combined with beam shaping techniques to enhance image quality in many applications [33].

Figure (2.2): Example B-mode ultrasound image [34].

2.6 Plane-Wave Imaging (PWI)

Plane-Wave Imaging (PWI) is an ultrasound imaging technique that allows for faster image acquisition and higher frame rates [35], [36]. In traditional ultrasound, to send and receive ultrasonic waves, beam focusing is utilized. However, in PWI to transmit and collect ultrasonic signals, a transducer's elements are all activated at the same moment to produce an unfocused beam [35], [36]. PWI can be used in medical diagnosis and non-destructive testing (NDT) in various industries [35], [37]. In medical diagnosis, PWI can produce high-resolution images through scan conversion and image reconstruction. PWI has various medical applications. Its main benefits are to rise the frame rate and decrease the number of elements required in the transducer array, allowing for ultrafast image collection, which is capable of imaging at kHz rates [35], [36]. Another application of PWI in the medical field is to measure the velocity of blood flow in the body [36]. This technique has also been used to improve Doppler images by filtering spatiotemporal clutter from ultrafast ultrasound data [36].

2.7 Ultrafast Ultrasound Imaging

Ultrafast ultrasound imaging is a technique that allows the analysis of rapidly changing physical phenomena in the human body, such as ultrasensitive flow imaging in the cardiovascular system or shear-wave elastography.

Ultrafast ultrasound, an acquisition technique that has been widely studied and applied over the last two decades, As the name implies, ultrafast ultrasound imaging can potentially exceed 1,000 frames per second by overcoming the conventional frame rate limitation which is usually much less than 1000 frames per second [10]. By delaying pulse times across a group of transducer elements, in transmission, conventional ultrasonography emphasizes the shape and steering of focused acoustic beams. To scan a 2D or 3D space, focused beams are transmitted and received line by line. This simple scheme, however, limits the frame rate to about 100 frames per second, which only meets the basic requirements of traditional medical applications. Un-focused acoustic waves, like limited diffracted, diverging, or plane waves, are transmitted in ultrafast speed to illuminate a broad-range space with a fewer number of beams. Ultrafast ultrasound has the ability to make an exceedingly high frame rate that exceeds 1,000 frames per second, because fewer beams are required to compose a single image frame. Implementing the ultrafast ultrasound concept has become feasible in the last two decades, thanks to the exponentially increasing computation ability. Due to the absence of transmission focusing, the advancement in frame rate in ultrafast ultrasound is detrimental to image quality.

To balance the ratio of frame rate to signal-to-noise ratio and resolution, Coherent compounding of steering plane waves has been shown to greatly increase both spatial resolution and signal-to-noise ratio, while still obtaining moderate-high framerates [10]. To improve image quality without introducing too much computational complexity, novel signal processing and beamforming techniques have been proposed.

The main difference between ultrafast ultrasound imaging and traditional ultrasound imaging is the high frame rates of ultrafast imaging, typically over 1 kHz, where traditional ultrasound imaging provides lower frame rates. This is because ultrafast ultrasound imaging requires only a single acquisition to reconstruct each image, while traditional ultrasound imaging typically requires multiple acquisitions to obtain sufficient image quality. Another difference is that ultrafast ultrasound imaging provides poor imaging quality due to unfocused beams, while traditional ultrasound imaging is focused, and it thus provides better imaging quality. In addition, ultrafast ultrasound imaging suffers from strong diffraction artifacts, mainly caused by grating lobes, sidelobes, or edge waves, while traditional ultrasound imaging does not have these artifacts. The high frame rate of ultrafast ultrasound imaging is the reason of using it to analyze rapidly changing physical phenomena in the human body [10].

2.8 Applications of Ultrafast Imaging

The basic principle of ultrafast ultrasound imaging was developed in the 1970s. However, practical applications of ultrafast ultrasound imaging only arise from the early 2000s.

The initial application of ultrafast ultrasound imaging was to visualize the propagation of a shear wave caused by an acoustic radiation force delivered by an ultrasonic push pulse. Other applications for functional imaging have been explored, such as blood flow imaging, heart function evaluation, and vascular viscoelastic characteristics [38].

2.8.1 Visualization of Blood Flow

There are two main types of blood flow imaging applications of ultrafast ultrasound imaging including vector flow imaging and Coronary Ultrafast Doppler Angiography (CUDA) [33].

2.8.1.1 Vector Flow Imaging

Color flow imaging is a technique for visualizing blood flow by measuring Doppler shifts and superimposing them on B-mode images. Flow patterns in circulation, on the other hand, are generally more complex, with vortices formed as blood passes via orifices such as the mitral valve. To image these more complex flow dynamics, different echocardiographic approaches have been developed. Doppler flow imaging is combined with Left Ventricle (LV) wall motion assessment using particle image velocimetry and vector flow mapping. However, both methods have intrinsic limitations due to low frame rates.

An innovative method based on ultrafast ultrasound combined with Doppler and speckle-tracking technology enables users to image complex blood flow without the use of contrast agents or mathematical hypotheses. This approach is less angle-dependent, allowing for two-dimensional imaging of blood flows in two dimensions without relying on wall motion assumptions, and has been validated for pediatric use on high frequencies curvilinear pediatric probes. The flow velocity data obtained can be used to compute energy losses, vorticity parameters, and intraventricular pressure gradients. However, challenges include large datasets, computational challenges, storage capacity limitations and penetration of ultrafast ultrasound plane waves [33]. Blood speckle-tracking techniques are projected to be more enhanced and, as technology advances, will probably replace present color Doppler techniques.

2.8.1.2 Coronary Ultrafast Doppler Angiography (CUDA)

Coronary ultrafast Doppler angiography is a nonsurgical technique that visualizes and quantifies distal periarteriolar coronary vessels using ultrafast ultrasound technology. This technique separates cardiac movement from blood flow using spatiotemporal filters, allowing reconstruction of vessel architecture and fluxes. Validated in human's models, CUDA can quantify coronary flow reserve, this makes it an effective noninvasive tool for detecting ischemic heart disease [39].

2.8.2 Visualization of Tissue Motion

Because of the availability of ultrafast ultrasound technology, more detailed, diverse applications for measuring heart function and tissue properties have been created. Shear wave imaging is one of the most sophisticated applications [33].

2.8.2.1 Shear Wave Imaging

Ultrafast ultrasonic technique catches tissue movements at extremely high frame rates. allowing for more detailed investigation of tissue motion. Various applications for evaluating heart function and tissue properties have been developed. One of the more advanced uses is shear wave imaging [33], [40].

2.8.2.2 Electromechanical Wave Imaging (EWI)

The direct association between electrical and mechanical activation that occurs between 20 and 50 ms depending on the cardiac region under examination is known as electromechanical coupling. As the muscles contract, electrical depolarization occurs, resulting in electromechanical activation. At the time of activation, the myocardium undergoes a transitory deformation that might be seen at very high frame rates. This information can be used to compute electromechanical activation times. The feasibility of this technology has been demonstrated in both 2D and 3D human patients [33], [41].

2.8.3 Tissue Structure and Fiber Orientation

In vivo myocardial fiber orientation was investigated utilizing diffraction-tensor MRI methods. However, recent work using ultrafast ultrasound has showed that imaging fiber orientation using ultrasound is feasible. Speckle echoes spatial coherence is used by Backscatter Tensor Imaging (BTI) to determine the direction of myocardial fibers; The spatial coherence is highest when fibers are parallel to the ultrasound wave. Shear wave velocities are utilized by Elastic Tensor Imaging (ETI) to construct fiber maps, which exhibit a good correlation with MR DTI using animal models. Despite this, clinical use remains a laborious process[42].

2.9 Cardiovascular Diseases Diagnosis

Ultrafast ultrasound has potential clinical applications in cardiovascular diseases, particularly for patients with congenital heart disease. Estimating Myocardial Stiffness (MS) has been shown to be promising as a measure of contractility and for detecting subclinical problems that standard approaches do not detect. MS has been proven in animal models to be a noninvasive indicator of cardiac contractility, while in humans, there are differences in end-systolic MS between healthy patients and those with amyloid. More geometric and load-independent systolic function metrics might be advantageous for patients with congenital heart disease, where morphology and loading are significantly varied [33].

2.9.1 Ventricular Function

Myocardial stiffness measurement is considerably more crucial in diastolic assessment, where stiffness and fling pressure assessment are the primary clinical issues. The majority of current echocardiographic diastolic assessment has been on early diastolic events impacted by myocardial relaxation. Early relaxation may not be significantly affected by diastolic dysfunction in children. Myocardial diastolic stiffness can be estimated noninvasively using shear wave imaging [33].

Myocardial diastolic stiffness has been demonstrated in humans to rise dramatically with age and excessively greater in patients with hypertrophic cardiomyopathy, hypertension-induced LV hypertrophy, and cardiac amyloidosis. Further validation and technical standardization will be needed before widespread clinical use becomes possible, but initial findings are promising [33].

2.9.2 Evaluating Coronary Perfusion and Cardiac Structure

Assessment of coronary micro perfusion is crucial for patients with congenital heart disease, as it may be relevant for certain congenital defects. Patients with reduced coronary perfusion and flow reserve are at increased risk of sudden death and have a reduced survival rate post-Fontan. Identifying patients earlier with reduced coronary perfusion and flow reserve could help stratify them and reduce the risk of sudden death. CUDA could replace postoperative coronary artery Doppler patterns by evaluating post repair coronary flow in 2D and assessing coronary flow reserve before leaving the operating room. Myocardial fiber orientation that can be visualized using ultrafast imaging plays a significant role in cardiac function, and abnormal fiber architecture in congenital heart disease and cardiomyopathies may predispose to decreased function. BTI could help understand the pathophysiology of congenital heart disease and offer potential for novel insights [33].

2.9.3 Electromechanical Rhythm Abnormalities

A previous research on cardiac fiber orientation has been primarily conducted on one-time vivo specimens utilizing diffraction-tensor MRI techniques. Recent research using ultrafast ultrasound shows that imaging fiber orientation by ultrasound is possible. Backscatter tensor imaging (BTI) determines cardiac fiber orientation by measuring the spatial coherence (i.e., the degree of similarity) of speckle echoes. The highest spatial coherence is found in fibers parallel to the ultrasonic wave, whereas the lowest is found in fibers at 90°. Myocardial fiber vectors can be constructed based on the degree of spatial coherence using this method. This has originally been proven in 2D and 3D models of heart tissue using fiber-reinforced composites, demonstrating that fiber orientation correlates with spatial coherence [43].

2.9.4 Future Directions Echocardiography

The imaging process used to examine both anatomy and functional assessment can take up to an hour or more. Multiple angles are used to image structures and hemodynamics and tissue motion measurements are performed using multiple methods. Color Doppler, tissue Doppler, chamber volumes, blood flow imaging, shear wave imaging, and tissue orientation may all be recorded in 3D and in a single acquisition with ultrafast ultrasound imaging employing simultaneous 4D image acquisition. The acquisition of multiple functional parameters simultaneously would lead to better measurement consistency and lead to new algorithms and indices for functional assessment. Ultrafast ultrasound has yet to be explored in the field of pregnancy.

Figure 2.3 shows a diagram that represents the most important clinical applications of ultrafast ultrasound imaging [33].

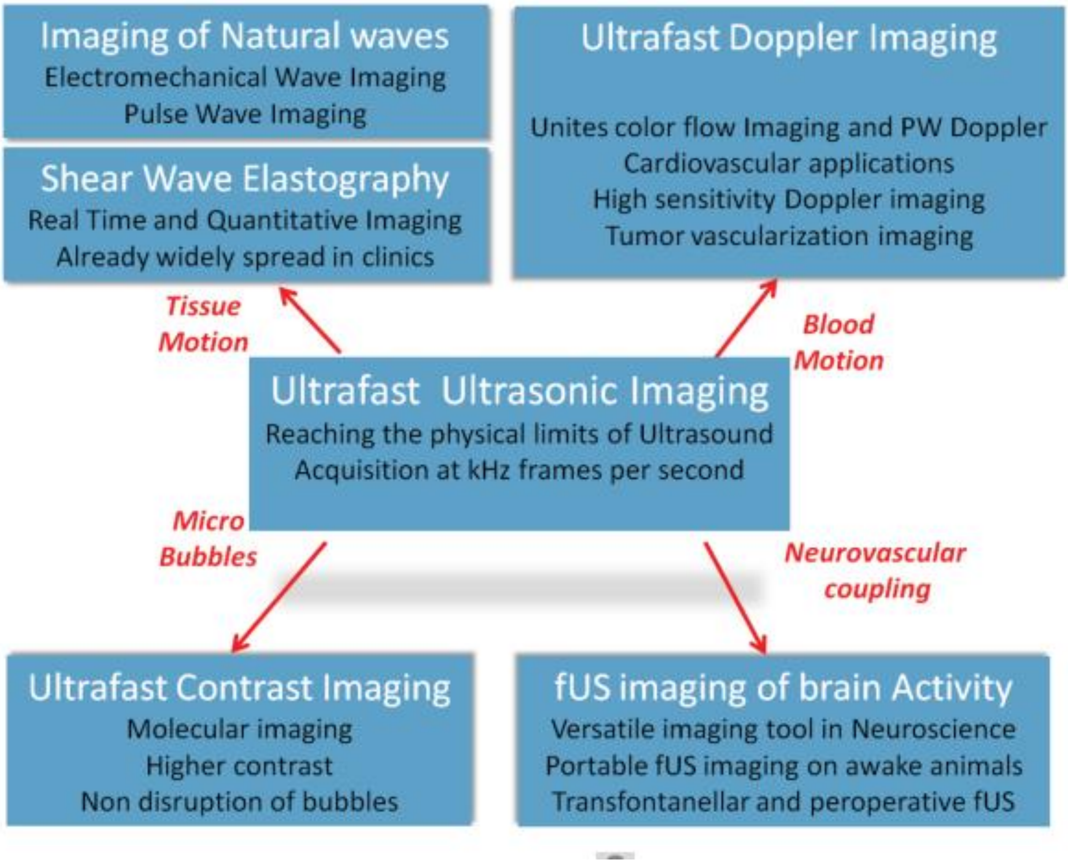

Figure (2.3): Clinical applications of ultrafast ultrasound imaging [44].

2.10 Limitations in Ultrafast Ultrasound Imaging

Ultrafast ultrasound is utilized in the preclinical phase for cardiology, with improvements in frame rate and spatial resolution. However, it remains imperfect due to challenges in tissue penetration, signal attenuation, and diffraction. Anatomical location of structures remains a challenge. For 2D flow quantification, the angle of sonification is crucial. Although new matrix array probes will enhance this, the current clinical use of ultrafast imaging is still limited despite the improvements in graphic and data processing [45].

2.11 Beamforming Principle

The basic operation in beamforming is to perform summation of the delayed data, received by the ultrasound transducer elements. In order to calculate the delays, the ray acoustics theory can be used. Figure 2.4 Explains the primary elements utilized in calculating focal delays. In this figure, the x value resembles the lateral distance, z is the axial distance (depth) and y resembles the elevation distance (third dimension).

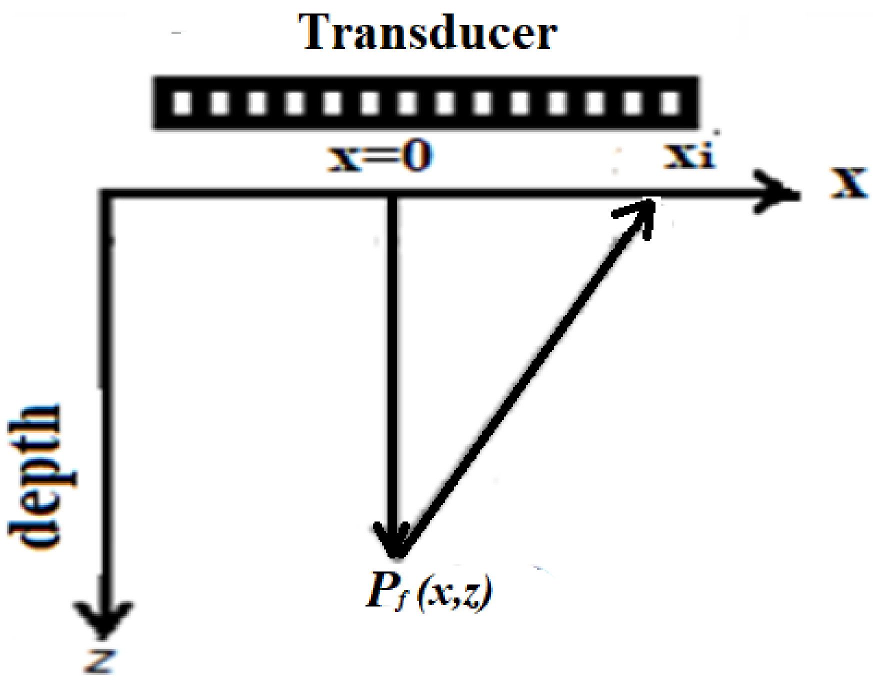

Figure (2.4): A diagram describing the round-off time required by a signal to travel to and reflect from a focal point.

To specify the sample value received from a focal point, it is necessary to know how long it takes the ultrasound beam to trip from the transducer to the point and then reflect back to the transducer element i. This can be done through knowing the distance of this journey, converting distance to time, and then simply dividing by the sampling time *Ts*. Assuming that the point position is $(x_f\ ,\ y_f\ ,\ z_f\ )$ and the center of the element's position is $(x_i,\ y_i,\ z_i)$, where the center of the transducer is situated at position $(x_0,\ y_0,\ z_0)$, then the transmit time in PWI (r_t) is calculated from the perpendicular space between the transducer and the point, which is equal to z_f, or simply the depth of that point. Distance (r_i) from the point to element i is calculated as follows [9]:

$$\boldsymbol{r_i = \sqrt{(x_i - x_f)^2 + (y_i - y_f)^2 + (z_i - z_f)^2}}. \qquad (2.1)$$

$(x_f\ , y_f\ , z_f\ )$ is the coordinate of the point position.

(x_i, y_i, z_i) is center of the element's position.

The central element of the transducer is situated at the position (x0, y0, z0), and its distance to the focal point, $\boldsymbol{r_c}$ is expressed as:

$$\boldsymbol{r_c = \sqrt{(x_0 - x_f)^2 + (y_0 - y_f)^2 + (z_0 - z_f)^2}}. \quad (2.2)$$

Thus, the delay needed to be applied to the i^{th} element data in order to compensate for the time of flight is equal to [9]:

$$\boldsymbol{t_i = \frac{1}{c}\, r_{total} = \frac{1}{c} * (r_c - r_i)}\,, \quad (2.3)$$

where c is the speed of sound in the medium, which is assumed in medical imaging to be 1540m/s [9]. Thus, the value of every point can be specified depending on the delays expressed in equation (2.2), but under the assumption of having a constant value of sound speed. The center of the transducer is assumed to be (0, 0, 0), while the value of the third dimension y equals to zero for all the points in traditional 2D B-mode images.

It can be considered in general that for a particular setup with an M-element ultrasound probe (M also refers to the number of the active elements in the transducer) and for the returning echoes recorded using the same ultrasound transducer, that each point in the (z, x) grid (for which y is equal to 0) will have a vector of values that are the delayed signals from each element. Therefore, a matrix of $(X\ , Z\ , M)$ is produced from beamforming, where summation will be performed over the third dimension and a single value will be assigned for each point in the final image. After this operation, the point values are normalized to the maximum, converted to dB scale, and then displayed as the final B-mode image points.

2.12 Data-Independent Beamforming

After applying focusing to the received data, different weights can be applied to this data. Beamformers can be either data-independent (fixed) or data-dependent (adapters) depending on the weights applied to the output array of the reflected signals. Delay and Sum (DAS) is the most fundamental data-independent beamforming, because of its simplicity and efficiency. It is common in medical ultrasound imaging, and very likely, the most spread beamformer in ultrafast ultrasound imaging. Before being employed for ultrasound imaging [46], [47], the technique of DAS has historically been used in ground-based and airborne radar as well as telecommunication [47], [48]. It is simple and can be parallelized due to its implementation. It is also fast and compatible with real-time applications, and due to being data-independent, it preserves the temporal coherence and statistical properties of the real envelopes [47], [49], [50].

DAS aims to create the image by delaying the incoming signal from each aperture channel then combining the resulting values. The apodization weights for the delivered signals are determined by the location of the receiving element. Signals from the central elements are given higher weights while those from elements farther from the center are given lower weights. Thus, all signals will coincide and then summation is performed [20].

The principle of PWI is illustrated in figure 2.5 on emit side. In emission, as in figure 2.5, each transducer element is responsible for controlling both the amplitude and time of excitation, such that the transmitted pulses are applied to all elements at the same time to produce an unfocused plane-wave.

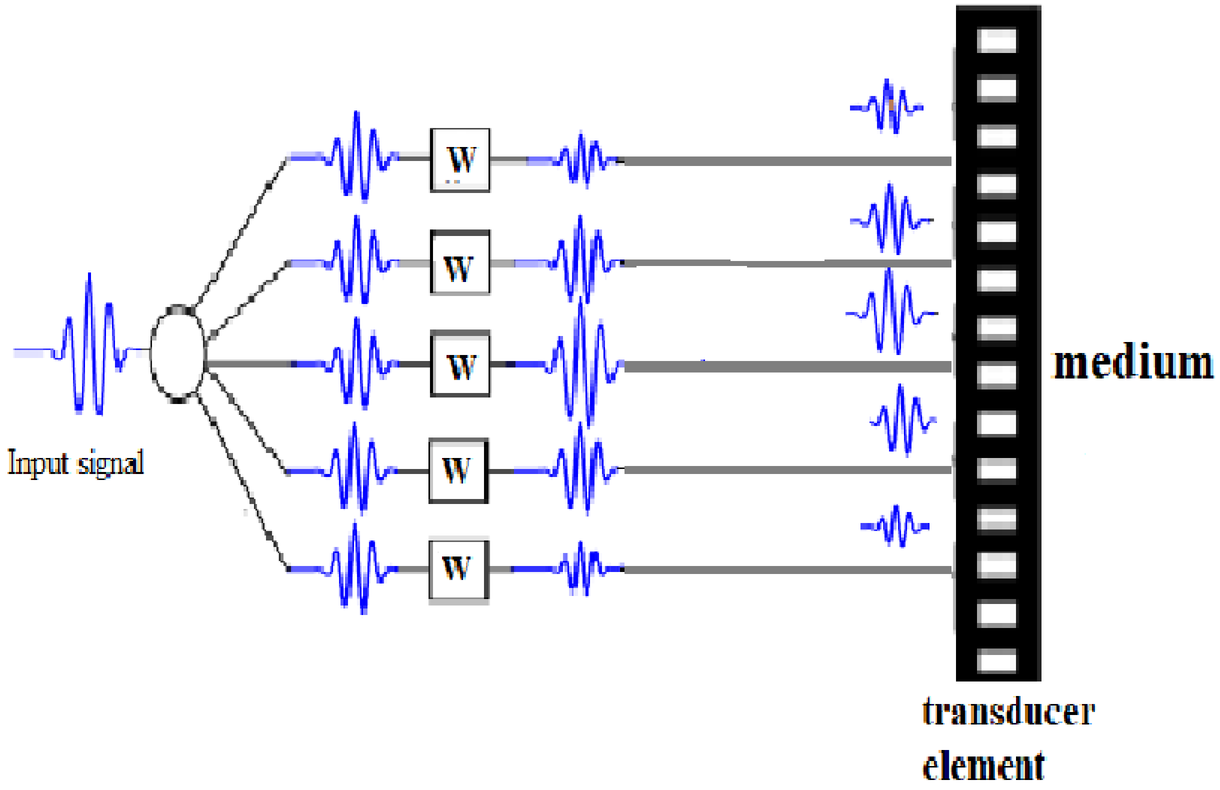

Figure (2.5): Transmission using PWI.

In reception, as shown in figure 2.6, the echoes received by the elements of the ultrasound probe, also called raw channel data, are focused (delayed) in order to compensate for the delays due to the time-of-flight differences. Then, the resulting signals are weighted using a weighting function, which is the receive apodization process. Afterwards, samples from each element are summed up to form the final beamformer output. Beamforming is more flexible in reception than in emission. In emission, once the elements have been excited, they cannot be controlled anymore during the process of beamforming. However, in receive, the raw channel data can be stored, and the weighting functions can be selected depending on the preferred characteristics of the recorded data, or according to the depth. The operation performed by DAS at each point $p(x, z)$ can be expressed as follows [51]:

$$\boldsymbol{P}(\boldsymbol{x},\boldsymbol{z}) = \sum_{\boldsymbol{i=1}}^{\boldsymbol{M}} \boldsymbol{p_i}(\boldsymbol{t} - \boldsymbol{\Delta t_i}), \tag{2.4}$$

p_i is represent, the value received by the receiving element i^{th}.

Δt_i is total round tip from transmitter to the received element.

To achieve perfect imaging quality, apodization is performed by decreasing the sidelobe level. Predefined and data-independent apodization weighting has the drawback of reducing the lateral resolution of DAS beamformer by widening the main lobe. Compared to conventional data independent beamforming, adaptive beamforming yields higher spatial resolution and lower sidelobe levels [20].

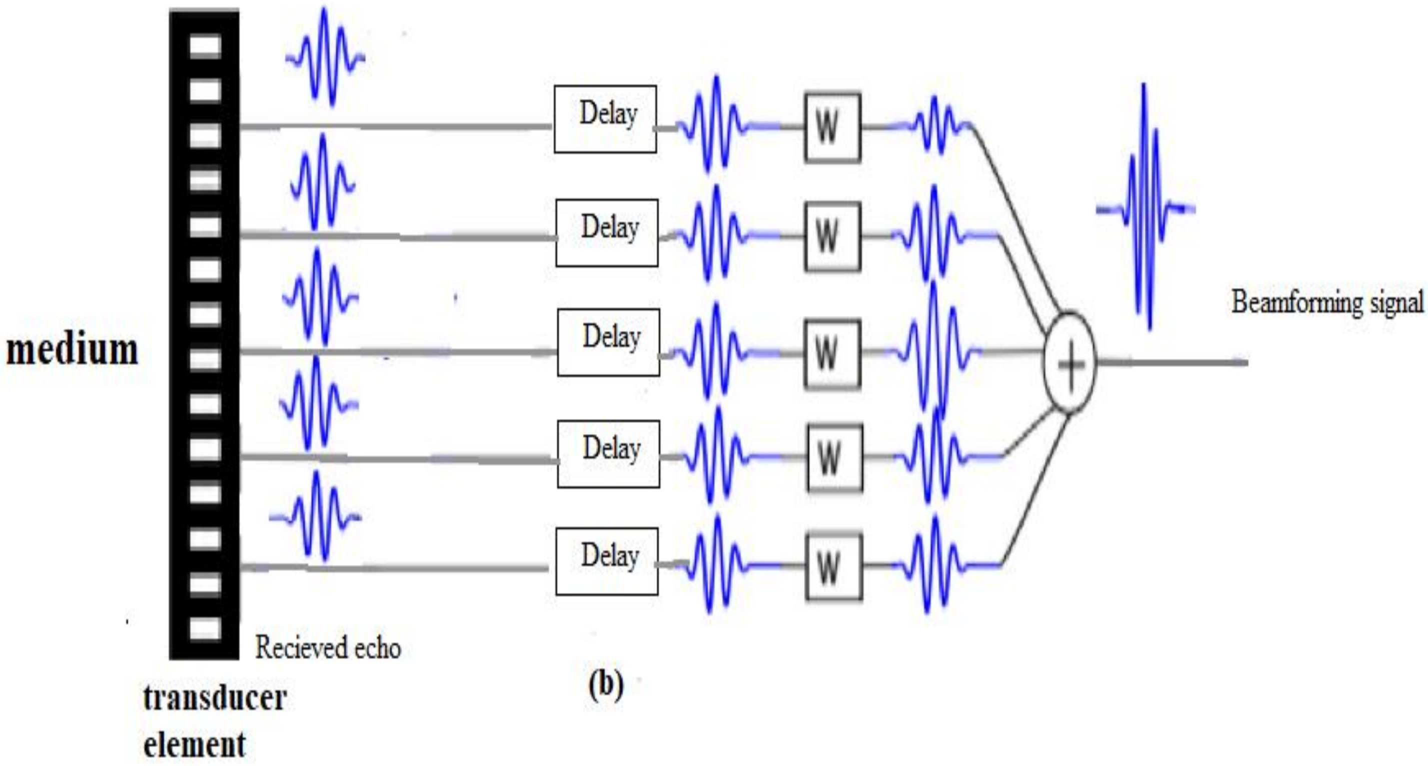

Figure (2.6): Delay and sum beamforming after reception.

2.13 Data-dependent Adaptive Beamforming

The operation of beamforming where output adapts according to the received echo data is called adaptive beamforming. Adaptive beamformers calculate the weights from the statistics of the received data in order to converge to an optimal response through the maximization of the produced SNR at the beamformer output [9]. Thus, the contributions of the noise and the signals that arrive from other directions than the desired direction are minimized. Figure 2.7 shows a diagram of reception operation and the calculation of the weighting in data-dependent beamforming.

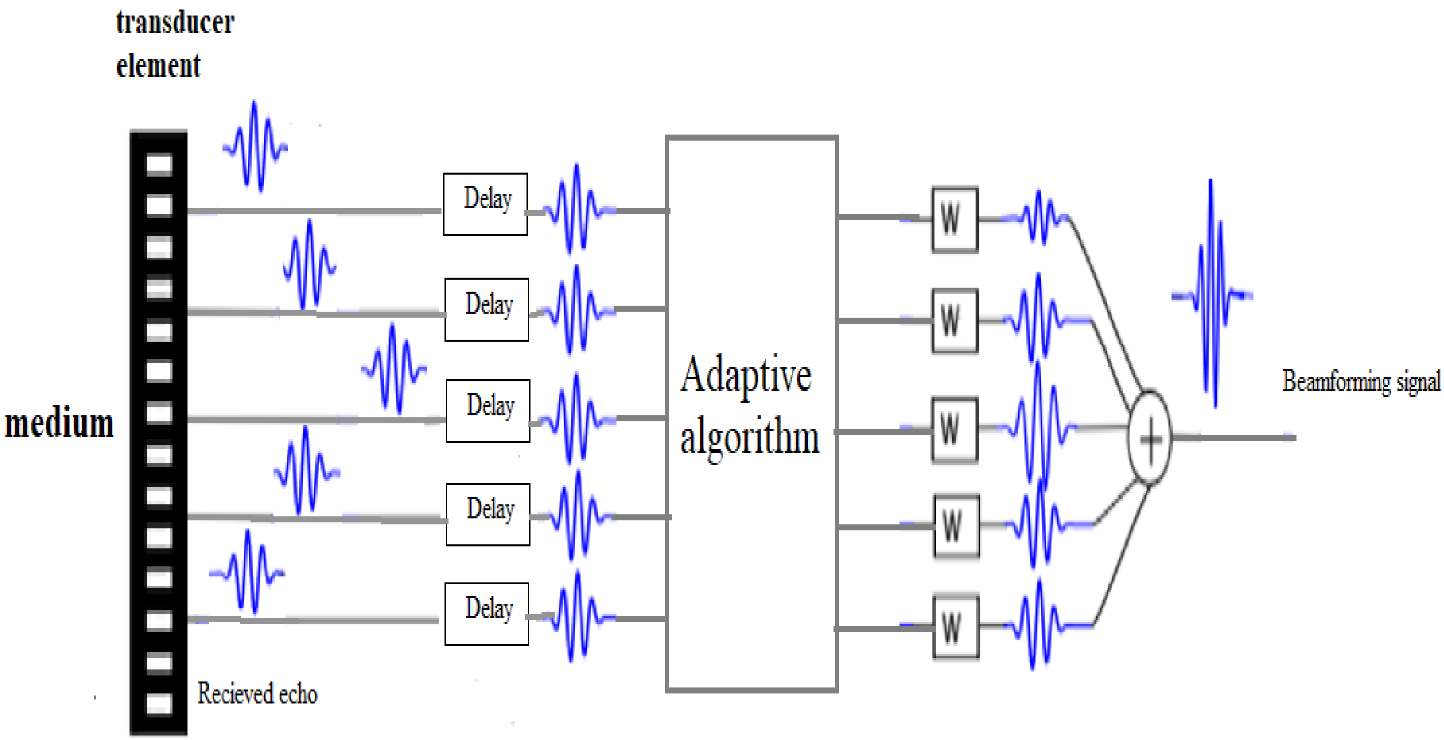

Figure (2.7): A diagram showing the principle of adaptive beamforming.

Adaptive beamformers have been employed in other applications of array signal processing, such as sonar and radar, for decades. The adaptive beamformer actively updates a set of apodization weights for each point in the image, whereas the standard beamformer has a passive procedure that uses precalculated data-independent apodization weights [52].

In the field of adaptive beamforming, there was a real and tangible pursuit by researchers and engineers, where the techniques rolled one after the other, and on top of these techniques or one of the widely used was the Minimum Variance (MV) Based Adaptive Beamforming.

2.14 Minimum Variance (MV)

MV beamformer is one of the widely used methods. It was originally introduced by Capon in 1969. MV beamforming is a signal processing technique that has been acquiring a wide interest by researchers in the medical ultrasound field [53], [54], [55], [56]. The Capon or Minimum Variance (MV) beamformer continuously updates the apodization weights, so that the variance (or power) of the weighted sensor signals is minimized under the constraint that the signal emerging from the point of interest is passed without distortion.

MV approach achieves higher spatial resolution than classic DAS, by lowering overall output power while maintaining the desired signals [56], or in other words, by keeping on-axis signals while minimizing off-axis ones [57], [58]. However, their execution usually imposes a significant computational load [59]. MV beamforming has been used to illustrate how adaptive methods' narrow beamwidth and low sidelobe levels can be used to improve resolution and imaging. The aim of MV is to apply an optimal set of weights in order to estimate the desired signal waveform as accurately as possible, while rejecting the interfering signals [54].

Synnevag *et al*. has highlighted the benefits of MV over DAS for producing higher contrast and resolution. They discussed methods that can improve robustness. They also demonstrated comparable quality levels while employing smaller apertures, fewer transmitted frequencies, or greater penetration depths.

The MV beamformer is used in conjunction with covariance matrix-based adaptive weighting. It could be used to enhance penetration depth while preserving lateral resolution [11]. The covariance matrix is critical in adaptive beamforming. It is a matrix that depicts the statistical relationship between the received signals of the array members.

The covariance matrix is computed through the received signals and then used to weight the array components in adaptive beamforming to improve the intended signal and minimize interference [60], [61]. Various techniques, such as interference-plus-noise covariance matrix estimation and sample covariance matrix estimation, can be used to estimate the covariance matrix.[61], [62].

The precision of the covariance matrix estimate can affect the quality of the adaptive beamforming process. Generally, the covariance matrix is an important component in adaptive beamforming since it allows for the strengthening of desirable signals while suppressing interference. However, MV beamforming does not increase contrast [63]. Researchers have proposed merging MV beamforming with other methods to increase contrast and to overcome this issue., such as Sign Coherence Factor (SCF) [58], [64], Coherence Factor (CF) weighting and Convolutional Neural Networks (CNN) [63].

Combining CF weighting with MV beamforming improves contrast and reduces sidelobes by enhancing in-phase signals while lowering out-of-phase signals [58]. Section 2.16 will introduce the CF concept.

The use of SCF could also modify the beamformer's input vector, which can reduce side lobe noise while requiring nearly no additional calculations [64].

The third proposed method of combining MV beamforming with CNN suppresses off-axis scattering signals while the MV beamforming apodization weights provide improved image resolution performance [63].

Researchers have also proposed combining MV beamforming with Phase Coherence Imaging (PCI) to enhance imaging resolution and contrast simultaneously. PCI analyzes phase dispersion, generates coherence factors PCF and SCF, and weighs the MV beamformed channel output [57].

Salari and Asl have proposed adaptively generated parameters for MV performance balance, ensuring user independence [65].

MV beamforming has two different types of implementations, in time domain and in frequency domain. In the use of time domain implementation, the weighting vector and output value for each point are derived by using vectors of data or sensor signals that have been received. In frequency domain implementing, Fourier transforms are used to convert sensor signals into the frequency domain. The final output is determined by taking the central sample of the result after applying the inverse Fourier transform to the weighted output vector. Time domain and frequency domain implementations of MV have close performance. Therefore, time domain implementation is usually selected because it requires less calculations and time.

The weighting vector in MV beamformer is always reorganized to minimize the output power by giving a unity value for the focal point's response. This criterion can be mathematically described as [66], [67], [68]:

$$\mathbf{w}_{\mathrm{MV}} = \arg \min_{\mathbf{w}} \mathbf{w}^{H}\mathbf{CM}\,\mathbf{w}$$

$$\text{subject to} \quad \mathbf{w}^{H}\mathbf{a} = 1\,, \tag{2.5}$$

The weighting vector is w,CM is the echo data's covariance matrix $\mathbf{w}^{H}$ is weight transpose. a is defined as the steering vector accustomed to recompense for the delays from the focal point for every element that is received. The final result of the weight value is displayed as [66], [68]:

$$\boldsymbol{w_{MV}} = \frac{\boldsymbol{CM^{-1}a}}{\boldsymbol{a^{H}CM^{-1}a}}\,. \tag{2.6}$$

The analytical form of CM is unknown, and it is typically estimated from the data. In spatial smoothing, the transducer array is subdivided into p subarrays, with one element being shifted between each two adjacent subarrays [69]. Temporal smoothing, where $(2K + 1)$ is a vector of specific number of samples for each focal point [70], is included in the CM calculation. The covariance matrix can be expressed as [66], [68]:

$$\boldsymbol{CM} = \frac{\boldsymbol{1}}{\boldsymbol{P}} \sum_{\boldsymbol{P}=\boldsymbol{0}}^{\boldsymbol{P}-\boldsymbol{1}} \boldsymbol{V_p V_p^H} \,, \tag{2.7}$$

where the number of subarrays is called p, and it is equivalent to $(M - Lp + 1)$. Lp is the length of the subarray in the spatial smoothing operation. The total amount of transducer elements is M. V_p is the p^{th} subarray, calculated as follows [66], [68]:

$$\boldsymbol{V_p} = \left[\boldsymbol{y_p(n)} \quad \boldsymbol{y_{p+1}(n)} \quad \cdots \quad \boldsymbol{y_{p+L_p-1}(n)}\right]', \tag{2.8}$$

where $y_p(n)$ is a portion of the input signal received by the p^{th} element, $p = 0, 1, \ldots, P-1$.

$y_p(n)$ represents a vector of length $(2K + 1)$.

The beamformer's output value is computed by multiplying the subarray average by the weighting vector, as follows [66], [68]:

$$\boldsymbol{Y} = \boldsymbol{w_{MV}}' \frac{\boldsymbol{1}}{\boldsymbol{P}} \sum_{\boldsymbol{p}=\boldsymbol{0}}^{\boldsymbol{P}-\boldsymbol{1}} \boldsymbol{V_p} \;. \tag{2.9}$$

By studying the effect of Lp on contrast and resolution in MV and method, it is observed that decreasing the value of Lp leads to lowering contrast ratio and contrast to noise ratio (approaching DAS beamforming method), and also decreases resolution and increases brightness, while the background speckle appears homogeneous and clear. On the other side, the increase in Lp value has a very positive and noticeable effect on resolution and contrast but at the expense of reducing the robustness of the method towards noise and off-axis signals.

In summary, MV offers improved resolution and adaptive capabilities, but it comes with high computational complexity and potential limitations in the overall image contrast.

2.15 Eigenspace-Based Minimum Variance Beamforming (ESBMV)

ESBMV is a technique used in medical ultrasound imaging to improve image quality. It is a type of adaptive beamforming that is used to suppress sidelobes, granting lobes and clutter in PWI [21], [71]. ESBMV was first introduced by Van Veen in (1988). It is based on the minimum variance (MV) beamforming algorithm, which is designed to improve image resolution in ultrasound imaging [71]. ESBMV overcomes the shortcomings of the MV algorithm by using eigenspace-based projection to estimate the covariance matrix [21], [71]. ESBMV method has been shown to improve the robustness of the algorithm with speckle pattern consistency and markedly remove noise while preserving the effective ability to suppress clutter and side lobes [72]. However, it usually introduces dark region artifacts alongside hyperechoic scatterers when obtaining improved contrast, which is called Black Box Regions (BBR).

Lately, several research groups have investigated and developed several ways to improve ESBMV beamforming. Mahloojifar and Asl have proposed an iterative ESBMV implementation for improving imaging parameter choices in a simulated cyst phantom. Zeng *et al.* suggested combining Wiener post-filtering with ESBMV to improve ESBMV resolution and contrast. Aliabadi *et al.* has developed a method for improving contrast in ESBMV by modifying the focal point value based on the qualities of the echo signals received by the surrounding points. Zhao *et al.* suggested an original technique that combines a coherence factor based on subarrays with ESBMV. This technique aids in the enhancement of imaging quality in terms of resolution, speckle homogeneity and contrast. Other techniques that have been proposed to improve ESBMV's performance include short-lag spatial coherence, DMAS beamformer, SCF, adaptive eigenvalue threshold and adaptive image quality. These methods aimed to remove BBR artifacts, reduce sidelobes, and improve signal-to-noise ratio. However, they had not totally remove ESBMV artifacts or noticeably improve imaging quality.

It is based on the minimum variance (MV) beamforming algorithm, which is designed to improve image resolution in ultrasound imaging [71]. ESBMV overcomes the shortcomings of the MV algorithm by using eigenspace-based projection to estimate the covariance matrix [21], [71]. ESBMV method has been shown to improve the robustness of the algorithm with speckle pattern consistency and markedly remove noise while preserving the effective ability to suppress clutter and side lobes [72].

In ESBMV, Signal and noise subspaces are found from the MV covariance matrix (CM), then the weight vector is projected onto the signal subspace. CM can be written as [15], [16]:

$$\boldsymbol{CM} = \boldsymbol{U \Lambda U^H} = \boldsymbol{U_S \Lambda U_S}^H + \boldsymbol{U_N \Lambda U_N}^H = \boldsymbol{CM_S} + \boldsymbol{CM_N}, \tag{2.10}$$

where the diagonal matrix is $\Lambda = \text{diag}\left[\lambda_1, \lambda_2, \dots, \lambda_{Lp}\right]$ CM's eigenvalues are represented by the diagonal of Λ, where $\lambda_1 \geqslant \lambda_2 \geqslant \cdots \geqslant \lambda_{Lp}$ are arranged in descending order. $U = [u_1, u_2, \dots, u_{Lp}]$ where u_i is the i^{th} orthonormal eigenvector for λ_i with $i = 1, \dots, Lp$. In this method, CM is divided based on its Eigen structure, into signal and noise subspaces. Subsequently, weighting vector in MV is subjected onto the corresponding subspace-constructed signal. As a result of the high coherency of on-axis signals, the energy produced by the mainlobe is focused on the eigenvectors related to the larger eigenvalues. Depending on this description, the signal subspace matrix (U_s) is written as [15]:

$$\boldsymbol{U_s} = [\boldsymbol{u_1}, \boldsymbol{u_2}, \dots, \boldsymbol{u_{Num}}] \, , \tag{2.11}$$

where Num is the number of eigenvectors included in the signal subspace. The signal subspace is constructed from the eigenvectors whose corresponding eigenvalues are greater than δ times the highest eigenvalue (λ_{max}), where δ is a value that can be set by the user from 0 to 1[13]. New weights are then calculated by projecting the MV weight to the signal subspace using the following equation [15]:

$$\boldsymbol{w}_{ESBMV} = \boldsymbol{U_S} \, \boldsymbol{U_S^H} \, \boldsymbol{w}_{MV}. \tag{2.12}$$

Where$\boldsymbol{U_S}$ is the signal subspace matrix.

H is denotes the transpose of the matrix.

In summary, ESBMV beamforming offers improved resolution and contrast, but it suffers from dark spots and BBRs artifacts which appear in background speckle.

2.16 Partial Eigenspace-Based Minimum Variance (PESBMV)

Contrast and resolution in MV adaptive beamformers are improved by ESBMV beamforming. Nevertheless, two types of artifacts reduce the overall image quality in ESBMV. Firstly, BBR around hyperechoic targets, and secondly dark spots in background speckle regions. Therefore, PESBMV was proposed to overcome those limitations. By depending on the value of Num, this method can distinguish or divide the image into two areas. The first area contains hyperechoic objects, wires (or point targets), and sidelobes, while the second area contains hypoechoic objects and speckle backgrounds. The weight in this method can be written as [20]:

$$W_{PESBMV} = \begin{cases} U_S U_S^H w_{MV} & \textit{if } Num > L_p.\eta \\ w_{MV} & \textit{otherwise.} \end{cases}, \qquad (2.13)$$

where η is a user-specified coefficient that is between 0 and 1. δ has a direct effect on the reduction of the noise level and Num. Depending on the type of the processed data the value of δ is selected, since it balances between imaging artifacts and the darkness and delineation of hypoechoic targets.

PESBMV was able to achieve a quantum leap in the PWI field by averting the BBR artifacts and controlling the dark spots through controlling the value of η. The ability of the factor Num in discriminating the imaging regions will be further clarified in chapter four.

In summary, PESBMV beamforming overcomes the limitation of ESBMV, by decreasing the BBR and sidelobes, with a little reduction in contrast.

2.17 Coherence Factor (CF)

CF is an adaptive method that measures the coherency of signals. It is also used to describe the superiority of adaptive imaging focusing [73]. The CF originally introduced as a method of quantifying the quality of ultrasound imaging. The use of CF is widespread to enhance imaging quality in both ultrasound and photoacoustic imaging [74], [75]. The ratio between the coherent and incoherent sums of the received signals after applying focusing delays [75]. CF is defined as [75] :

Where:

$x_i(k)$ represents the data received from channel i after applying focusing delays

k is the time index.

M number of elements.

$$\boldsymbol{CF(K)} = \frac{\left|\sum_{i=0}^{M-1} x_i(k)\right|^2}{M\sum_{i=0}^{M-1} |x_i(k)|^2}\ , \tag{2.14}$$

In ultrasonic imaging, CF value is commonly utilized as a weight to eliminate sidelobes. By using coherent signals, the value of CF increases, allowing the beamformer output to pass with no distortion. On the other hand, the beamformer output is attenuated by incoherent signals, which lowers the value of CF. By utilizing this property in the CF, artifacts and sidelobe levels can be reduced, and spatial resolution can be enhanced in point target imaging. The ultimate beamformed output is found by multiplying the CF by the final beamformer output.

By computing the CF for each image point and then multiplying it by the beamformer output at that point, the CF can be used to adaptively weight the output of any form of beamformers as shown in figure 2.8. Despite those advantages of CF, there are two main disadvantages of using this type of adaptive weighting. Firstly, due to its high sensitivity to incoherency, the CF cannot maintain the homogeneity of speckle-generating targets, which results in reducing the intensity level and increasing the variance in background tissue. Secondly the generation of BBR artifacts on the sides of hyperechoic targets in the region of interest. The incoherence created by the sidelobes of the lesion that intersect in this area produces artifacts, that diminish the value of the CF [75].

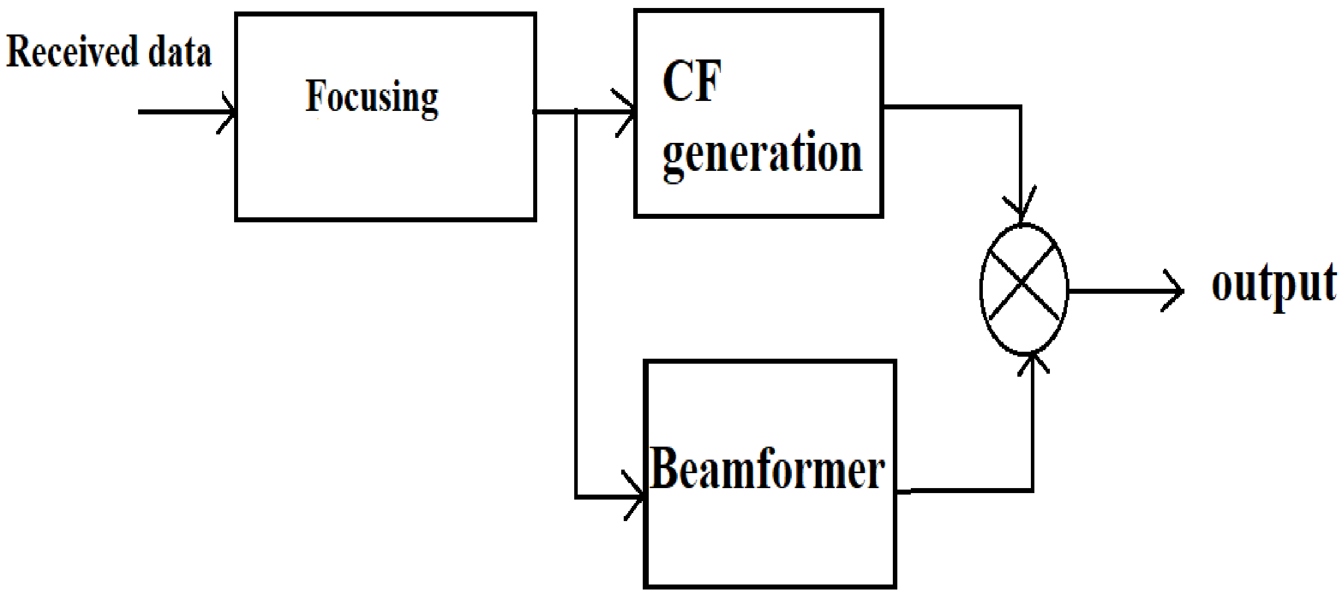

Figure (2.8): Block diagram of coherence-weighted beamforming using CF [76].

In summary, the advantages of coherence factor beamforming include high enhancing resolution, despite the distortion which is usually introduced in background speckle by dark spots and BBRs.

2.18 Wiener Post Filter

The Wiener post-filter, also known as the Wiener filter, is a signal processing filter that uses linear time-invariant (LTI) filtering of an observed noisy process to give an estimate of a desired or target random process, assuming known stationary signal and noise spectra, and additive noise. In ultrasound imaging, the Wiener filter is a denoising technique used to minimize speckle noise and improve image quality. It is a universal filter that minimizes the mean square error between the estimated and the original signal to give an estimate of the uncorrupted signal [77].

$$\boldsymbol{H}_{\boldsymbol{Wiener}} = \frac{|\boldsymbol{Y}|^{2}}{|\boldsymbol{Y}|^{2}+\boldsymbol{w}^{\boldsymbol{H}}\boldsymbol{CM}_{\boldsymbol{n}}\boldsymbol{w}} \tag{2.15}$$

where $w^{H}CM_{n}w$ represents the noise of the output power, with *w* being the weight of the used beamformer.

CM_{n} is the noise covariance matrix for the used beamformer.

$|Y|^{2}$ represented the power of the output signal of the used beamformer.

The noise covariance matrix is obtained by the following equation.

$$\mathbf{CM_n} = \frac{\mathbf{1}}{\mathbf{M}}\sum_{\mathbf{i=1}}^{\mathbf{M}} (\mathbf{x_i}(\mathbf{k}) - \mathbf{Y}(\mathbf{k}))^{\mathbf{2}} * \mathbf{I} \tag{2.16}$$

where $x_{m}(k)$ the signal received by the i^{th}element. I is Identity matrix.$Y(k)$ is the power of the output signal of the used beamformer.

In summary, the Wiener post-filter offers optimal noise reduction and adaptability but requires prior knowledge and may lead to over-suppression of artifacts in certain scenarios.

2.19 Standard Deviation

In statistics, the standard deviation is a measure of the amount of variation or dispersion of a set of values. It tells how spread out from the center of the distribution the data is on average. A low standard deviation indicates that the values tend to be close to the mean of the set, while a high standard deviation indicates the opposite. The standard deviation is calculated as the square root of the variance. The standard deviation is calculated using the formula [86]:

$$\boldsymbol{\sigma} = \sqrt{\frac{\sum_{k=1}^{M} (\boldsymbol{x}(\boldsymbol{k}) - \boldsymbol{\mu})^2}{\boldsymbol{M}}} \quad . \tag{2.17}$$

Where μ is the mean value.

$x(k)$ is represent the received data.

M is represent number of elements.

CHAPTER THREE

SIMULATION -BASED EVALUATION OF PROPOSED METHOD

3.1 Introduction

This chapter displays the suggested method and its flowchart, as well as investigating the proposed method and other beamformers performance by applying them to point spread function simulations. The obtained results are also discussed in this chapter.

3.2 Proposed Method

The method proposed in this work aims to maintain high imaging quality via discriminations between the different areas of an image. Rather than discriminating the image region into two groups of areas as in PESBMV, the proposed method further discriminates the image so that four different image areas are distinguished from each other. This is done relying on the Num value as well as the weight of ESBMV method. This method is proposed to take advantage of the positives of ESBMV, MV and CF, each in the most suitable region, where the most suitable beamformer is applied.

Thus, the idea is exploiting the positives of a number of beamforming methods, where depending on specific values that detect different areas in the image, the best performance of the methods is included in each region to obtain high-quality images.

Initially, two factors are proposed to distinguish between the different areas of the image. The first parameter is the value of Num that is the number of vectors in the signal subspace matrix produced by the ESBMV technique. By using this factor, image can be divided into two regions. The first region includes hyperechoic targets, point targets (or wire points) and sidelobe regions, where the value of this factor is found to be less than its half maximum possible value, which is the subarray length (Lp).

The second area distinguished by *Num* is the hypoechoic targets and background speckle, where it is found that the value of *Num* is above half the subarray length (L_p) . This behavior of *Num* is shown in figure 3.1 and figure 3.2, on two different in-vitro data sets. The objects included in the areas for which these two data sets are taken is shown in (a) for figure 3.1 and figure 3.2. The value of L_p used during producing this figure is 32. This is proved previously in PESBMV method, where the use of ESBMV is blocked in the first area and allowed in the second area. In this way, BBR artifacts are prevented from occurring at the side lobe regions and dark spots are reduced in many points in the background speckle.

Afterwards, the role of the method proposed in this work comes through further discriminating each of the two areas into other two subareas. This gives flexibility in the use of different types of beamforming in each of the four regions, allowing for further improvement in imaging quality. This discrimination is performed by depending on *Num* value, where it is found, as can be clearly seen in (b) for both figure 3.1 and figure 3.2, that *Num* can distinguish between the elements in the first region (including hyperechoic and point targets and sidelobes), by giving values of larger than 1 to sidelobes and 1 to hyperechoic and point targets. It is also found that the weight produced by ESBMV method can very well distinguish between the elements of region two (which includes hypoechoic targets and speckle backgrounds), by giving dark values to hypoechoic targets that are very distinguishable from the bright values given to the speckle background.

After discrimination, the proposed method uses four different types of beamforming techniques in each of the four regions as follows. Firstly, ESBMV $(Lp = M/2)$ multiplied by CF is used where hypoechoic targets exist. Secondly, MV$(Lp = 1)$ is used at the background speckle and hyperechoic target regions. Finally, MV$(Lp = M/2)$ is used for areas that include BBRs resembled by the sidelobe regions. The flow chart that explains the steps followed by this method is shown in figure 3.3.

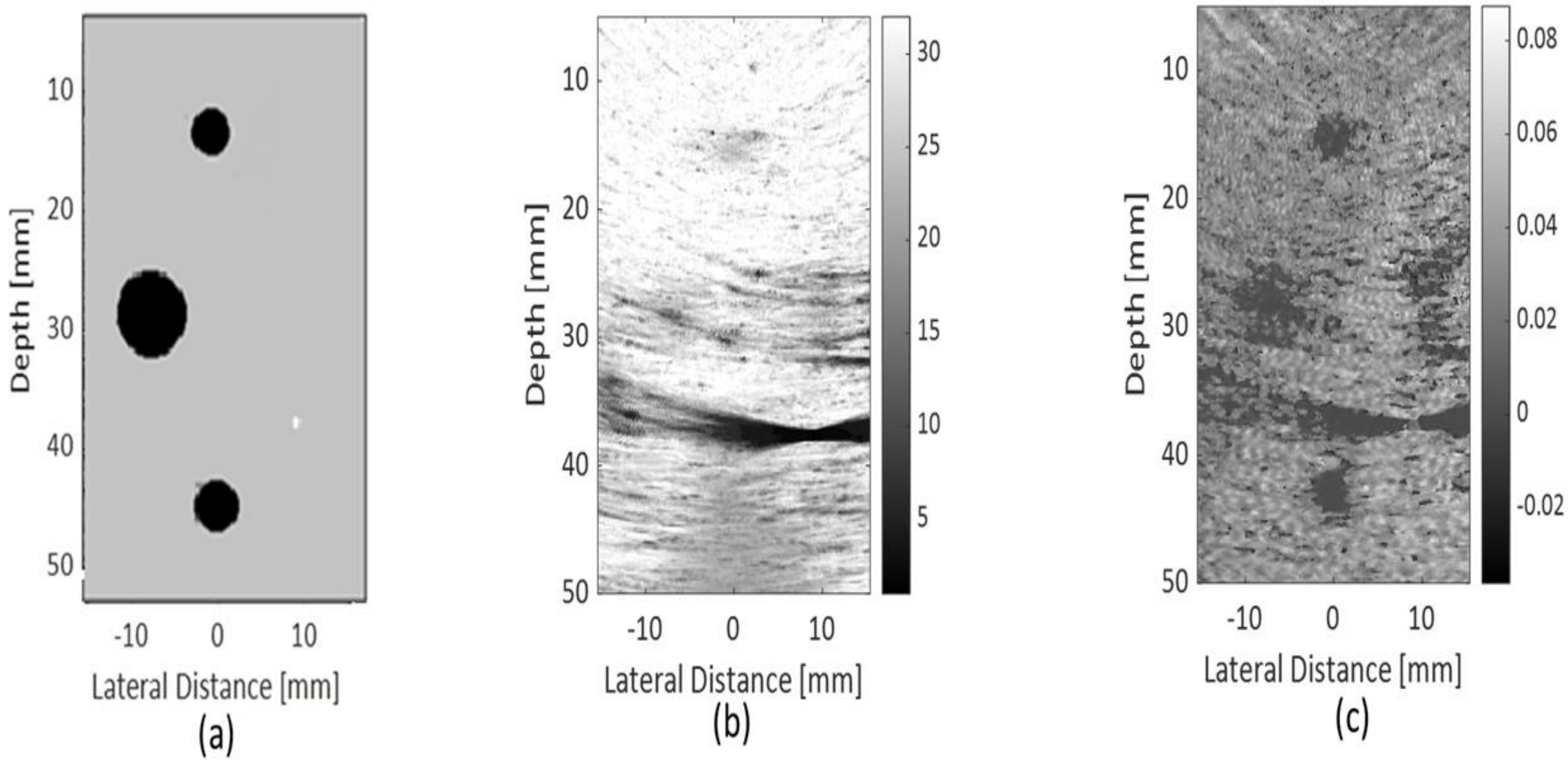

Figure (3.1): The value of *Num*, using reference ESBMV at (δ= 0.2, $L_p = 32$) in (b) for the contrast phantom shown in (a). (a) is a contrast phantom with three cysts centered at the 15 mm, and 42 mm depths. (c) show the weight of ESBMV at (δ= 0.2,$Lp = 32$) using contrast datasets.

Figure (3.2): The value of *Num*, using reference ESBMV at (δ= 0.2, $L_p = 32$) in (b) for the resolution phantom shown in (a) . (a) is a resolution phantom with 7 wires and a hyperechoic lesion at a depth of 28mm. (c) show the weight of ESBMV at (δ= 0.2 ,$Lp = 32$) using resolution datasets.

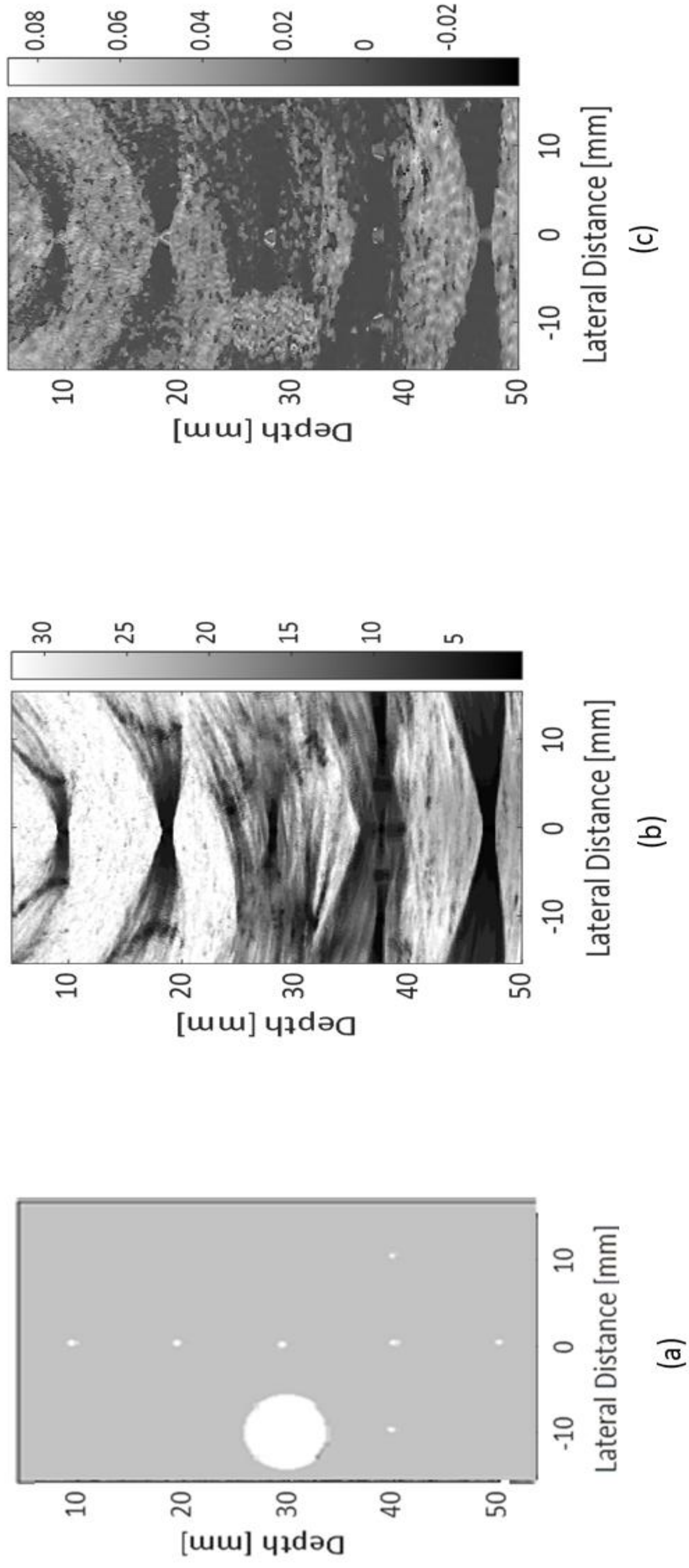
Depth [mm]
Lateral Distance [mm]
(a)
(b)
(c)

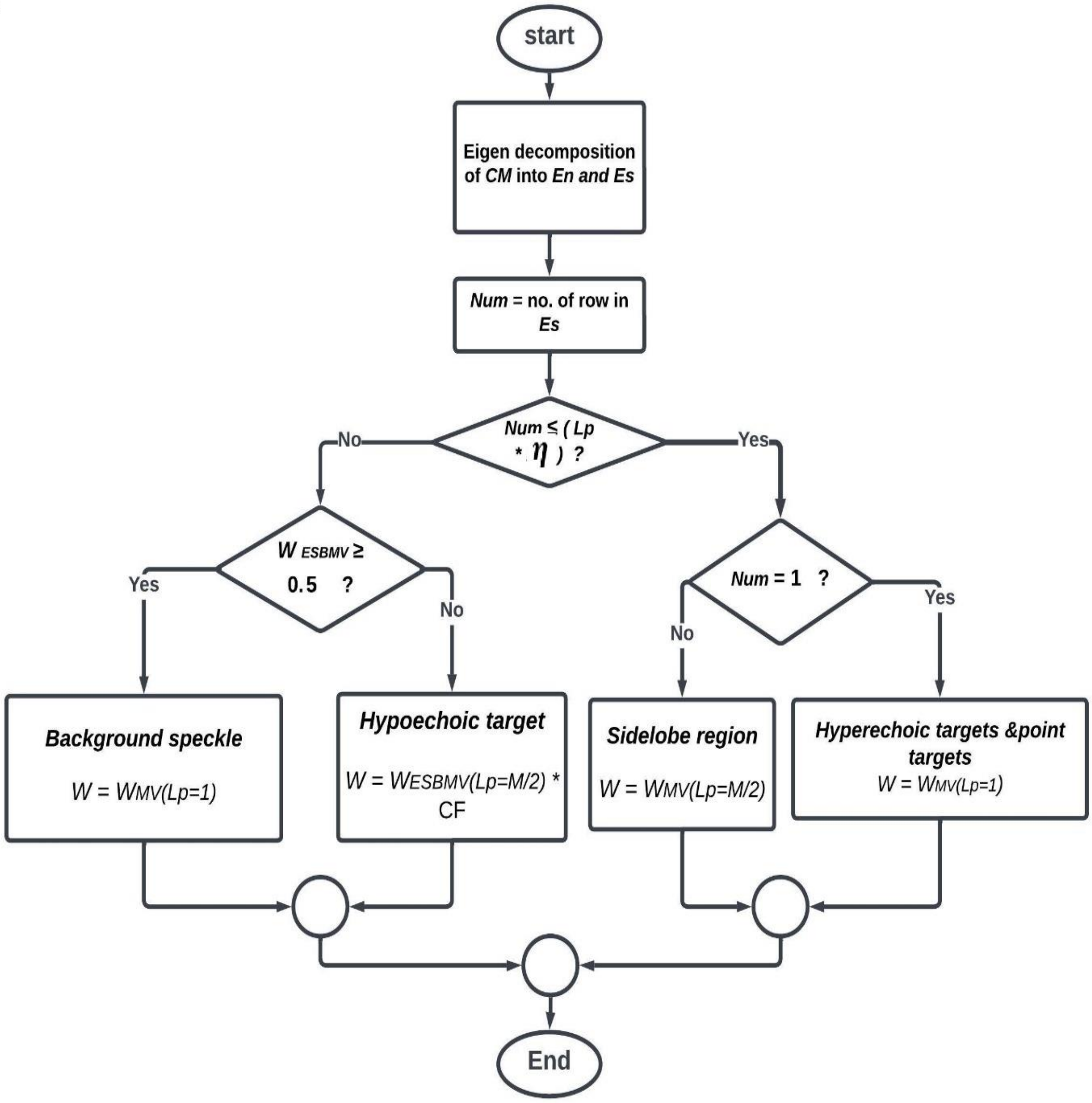

Figure (3.3): Flow chart outlining the steps followed by the proposed method.

3.3 Differences Between PESBMV and the Proposed Method

The main difference between the proposed method and PESBMV is look like by the levels of image discrimination. PESBMV includes a single level of discrimination that divides image structures into two regions, while the proposed method further discriminates each of these two regions into two subregions, allowing for the use of four types of beamforming methods instead of only two.

PESBMV has been mainly proposed to minimize the artifacts of ESBMV resembled by BBRs and dark spots, without adding improvement to image quality. Unlike PESBMV, the proposed method adds another level of image decomposition so that image quality can be improved without reducing the ability of the method to reduce artifacts.

Another difference between PESBMV and the proposed method is the dependence of the proposed method on a new discrimination factor (ESBMV weight), in addition to *Num* used in PESBMV. Figure 3.4 shows a comparison between the flow charts of the two methods,

PESBMV and the proposed method.

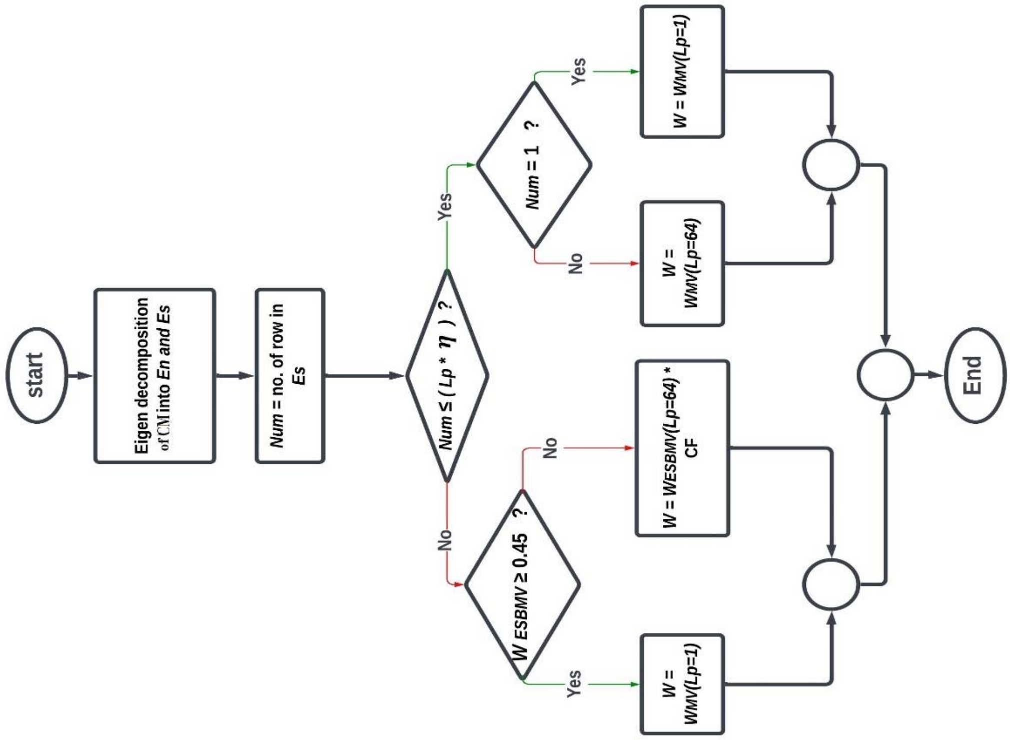
start
Eigen decomposition of CM into En and Es
Num = no. of row in Es
Num ≤ (Lp * η) ?
Yes
No
Num = 1 ?
W ESBMV ≥ 0.45 ?
W = WMV(Lp=1)
W = WMV(Lp=64)
W = WESBMV(Lp=64) * CF
W = WMV(Lp=1)
End

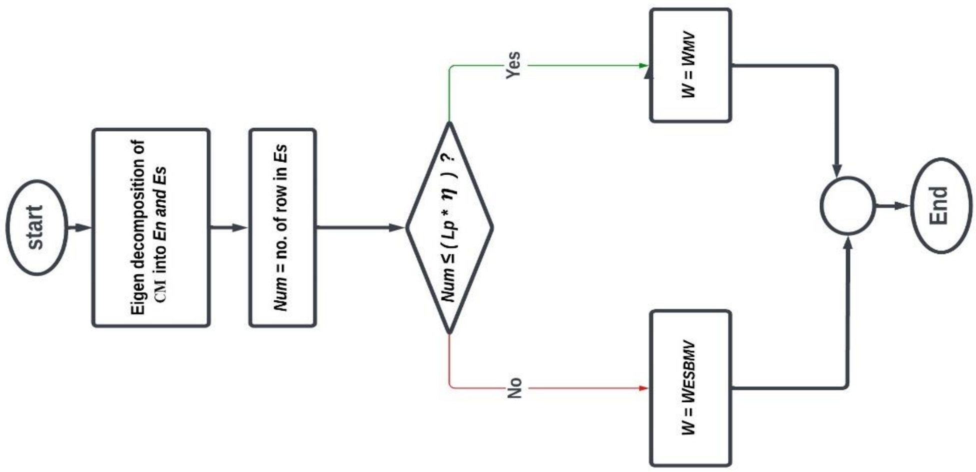
start
Eigen decomposition of CM into En and Es
Num = no. of row in Es
Num ≤ (Lp * η) ?
Yes
No
W = WMV
W = WESBMV
End

3.4 PSF Imaging Using Field II Simulation Program

Point spread function (PSF) imaging is commonly used to evaluate the imaging quality of an ultrasound systems, by displaying the spatial impulse response of the ultrasound system. [82]. The PSF images result from imaging point targets located in various locations in the imaging area. The main property measured for PSF is spatial resolution, which is defined as the width of the mainlobe at the center of PSF along lateral, axial or elevational direction, after a specific drop in amplitude from the peak value. In addition to spatial resolution, the pattern of side lobes and grating lobes can also be assessed using PSF imaging [82]. Thus, PSF is often analyzed to determine the image quality of an ultrasound systems and algorithms.

The formation of PSF is determined by several practical factors such as the transducer aperture, element directivity, apodization, pitch, imaging position and steering angles. Conventional numerical simulations are usually used to provide the ability to examine those factors' effects and produce empirical expressions based on PSF performance.

Field II simulation software is one of these simulators. Field II is a software that uses linear acoustics to simulate ultrasonic translator fields and ultrasound imaging. It was created at Duke University in 1991-92 and has been available for free download since 1995. The program calculates pulsed ultrasound fields using the Tupholme-Stepanishen approach and is capable of estimating emission and pulse-echo fields for both pulsed and continuous wave scenarios for a wide number of various transducers.

The software allows users to simulate ultrasonic transducer fields and ultrasound imaging, making it a powerful tool for learning and creating novel ultrasound imaging techniques.

The program comes in a variety of variants, including MATLAB, Octave, and C library versions, making it compatible with a variety of programming environments and systems. Field II can be downloaded for free.

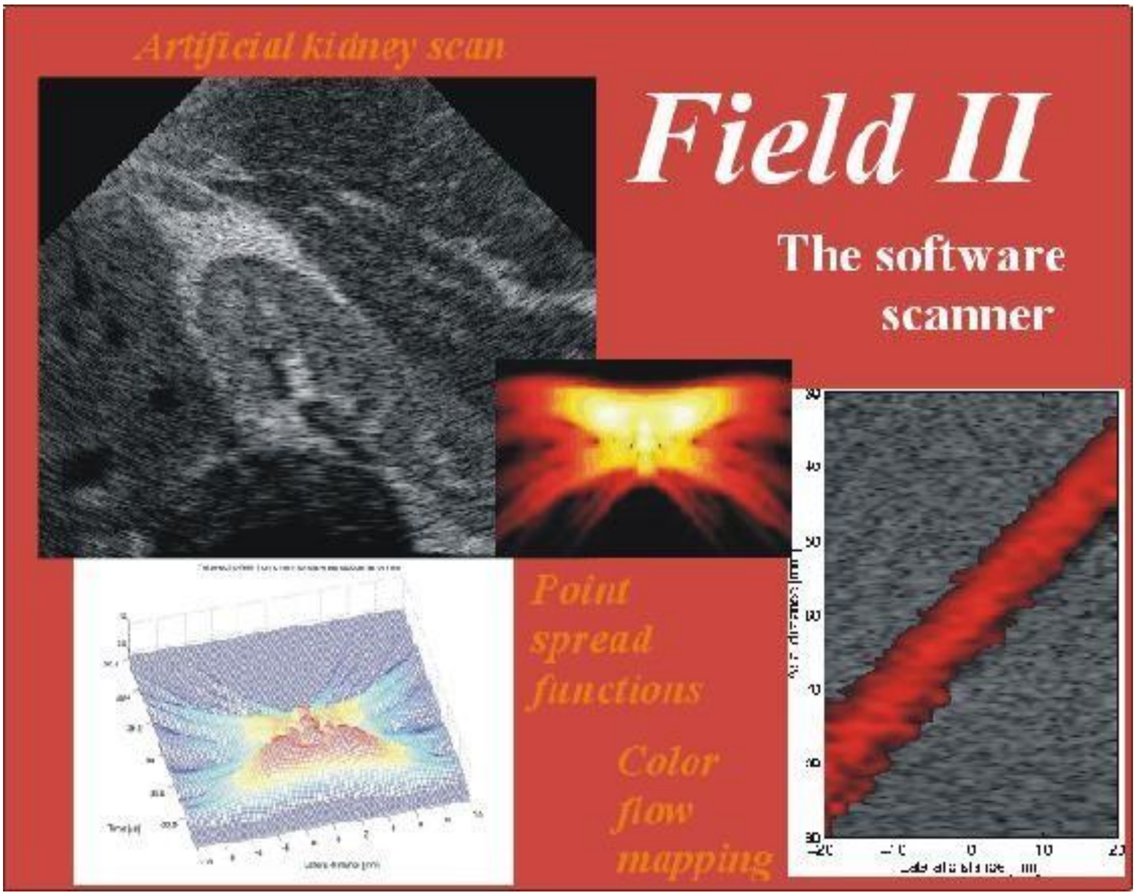

Figure (3.5): Field II simulation program initialization background [78] .

3.5 Specifications of Simulated System

A linear array consisting of 128 elements with a width of 0.27 mm, a height of 6.0 mm, and a pitch of 0.304 mm is simulated. The central frequency of the transmitted sinusoidal pulse is 6 MHz, with 100% bandwidth, and 100MHz sampling frequency. All 128 elements are used during the transmission and reception, with no focusing at the transmission and dynamic focusing at the reception. The sinusoidal wave consists of 2.5 cycles. A medium sound speed of 1540m/s is assumed.

3.6 Quality Metrics

This work employs well-known quality metrics for the quantitative analyses of the performance of the proposed method. Those metrics are Contrast-to-Noise Ratio (CNR), Contrast Ratio (CR), Full Width at Half Maximum (FWHM), and Speckle signal-to-Noise Ratio (SSNR).

As indicated in the following equation, CR is calculated to evaluate imaging contrast from the absolute difference between the cystic area's mean value and the background tissue mean value [83]:

$$\boldsymbol{CR} = |\boldsymbol{\mu_i} - \boldsymbol{\mu_b}|, \tag{3.1}$$

where the mean values within the cyst target and speckle are μ_i and μ_b, respectively. CNR is another measure of contrast that is found as follows [83]:

$$\boldsymbol{CNR} = \frac{|\boldsymbol{\mu_i} - \boldsymbol{\mu_b}|}{\sqrt{\boldsymbol{\sigma_i^2} + \boldsymbol{\sigma_b^2}}}, \tag{3.2}$$

where σ_i and σ_b are the equivalent standard deviations, within the cyst target area and the speckle background area, respectively. In the contrast dataset, two 2x1 mm rectangles inside the two cysts at the center of the image, with two 11x15 mm rectangles to the left and right top corners of the image are the areas for which CR and CNR are calculated depending on equations 3.1 and 3.2.

Background Speckle Signal-to-Noise Ratio ($SSNR_{\mathrm{Bg}}$) is used to evaluate the quality of background speckle. The following formula is used to determine $SSNR_{\mathrm{Bg}}$ [84], [85]:

$$\boldsymbol{SSNR_{Bg}} = \frac{\boldsymbol{\mu_b}}{\boldsymbol{\sigma_b}}\ , \tag{3.3}$$

In contrast dataset, an 11 x 17 mm rectangle in the right top corner is used to measure the background speckle's homogeneity using $SSNR_{\mathrm{Bg}}$. A similar formula to that used in equation 3.3 is used to calculate the BBR's Speckle Signal-to-Noise Ratio ($SSNR_{\mathrm{BBR}}$) as follows [84], [85]:

$$\boldsymbol{SSNR_{BBR}} = \frac{\boldsymbol{\mu_{BBR}}}{\boldsymbol{\sigma_{BBR}}}, \tag{3.4}$$

where μ_{BBR} and σ_{BBR} are the BBR's standard deviation and mean values, respectively. In the resolution phantom, two 2x2 mm squares to the sides of the point target at a depth of 9mm indicates the area for which, BBR artifacts are evaluated using $SSNR_{\mathrm{BBR}}$.

3.7 Simulations of PSF Imaging

The PSF module simulated in Field II consists of three-point targets located at depths, 30 and 35 mm, perpendicular to the middle of the transducer (x=0). Lateral resolution is assessed for the point at 30 mm depth.

Ultrasound images of this PSF model were produced using different beamforming methods, and the resulting B-mode images are as illustrated in figure 3.6. The images in this figure are all produced with a dynamic range of 60dB.

In figure 3.6 image (a) shows the result of using MV beamforming at subarray length of 32. In figure 3.6 (b), ESBMV beamforming is used with subarray lengths of 32. Finally, images (c) and (d) in Figure (3.6) show the results of using PESBMV beamforming and the proposed method respectively, the beamforming performance at the 30 mm depth was evaluated in terms of sidelobe levels and resolution using Full Width at Half Maximum (FWHM), where calculating the FWHM at 6 dB drop from the peak of the main lobe in the lateral direction gives the lateral resolution [79]. FWHM measurements are given in Table (3-1).

Figure 3.6 show that PESBMV has a main lobe equivalent to MV ($Lp = 32$). Image quality in ESBMV compared to MV ($Lp = 32$) is slightly improved, as shown in figure 3.6 (a, b). according to this figure, it can be confirme that ESBMV-based methods have better lateral resolution compared to MV methods. The sidelobe and FWHM are both improved when using the proposed algorithm compared to the other simulated beamformers. Figure 3.7 shows the lateral profile of the four simulated beamformers, for the point centered at the 30 mm depth. This figure shows that the proposed method is superior inside lobe reduction and in resolution value, compared to the other simulated beamformers.

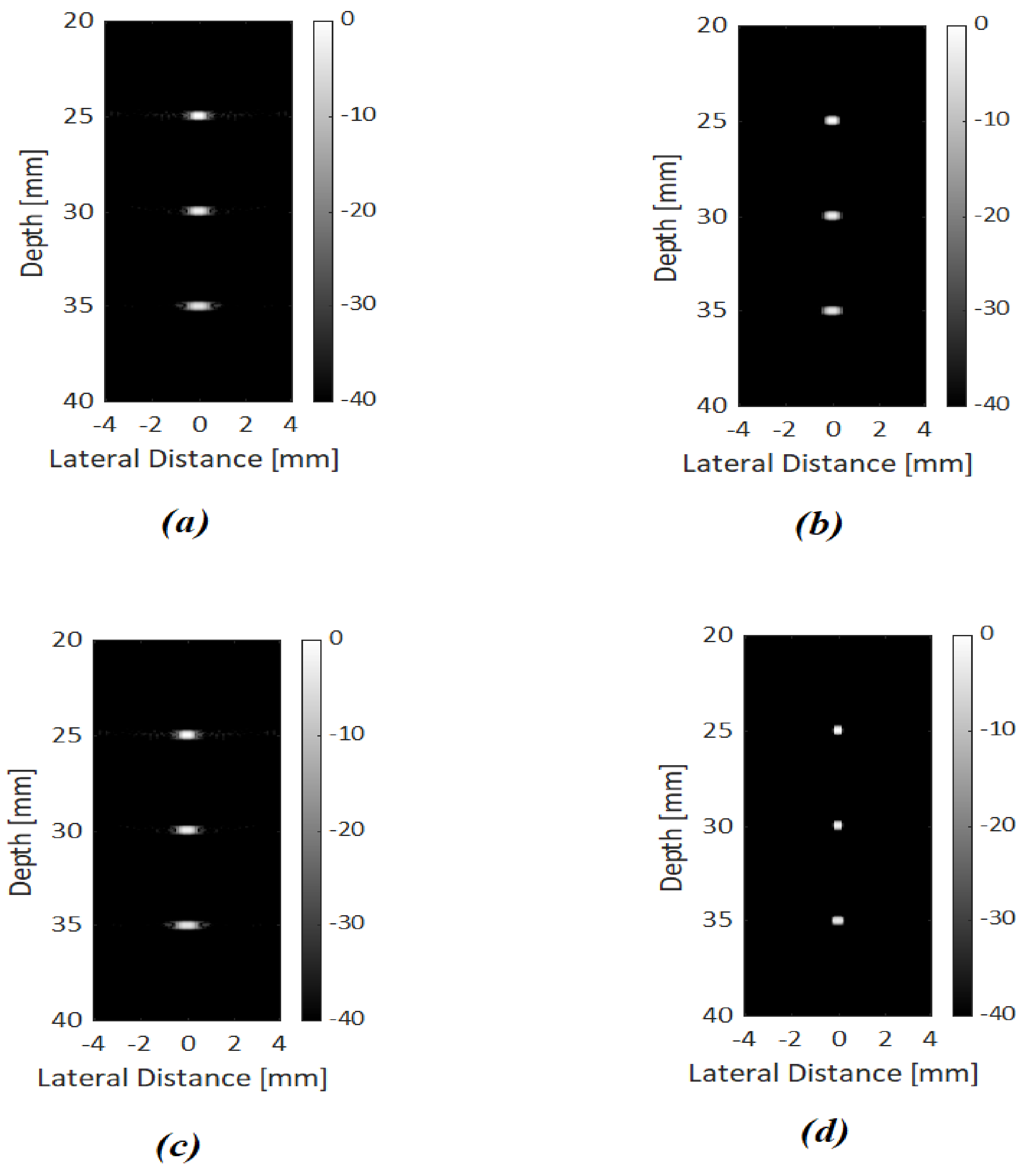

Figure (3.6) :Simulated point targets using beamforming methods: (a) MV (Lp = 32) (b) ESBMV (δ = 0.2 , Lp = 32) (c) PESBMV (δ = 0.2, η = 0.5, Lp = 32) (d) proposed method (δ = 0.2, η = 0.5). All images are shown in a dynamic range of 60 dB.

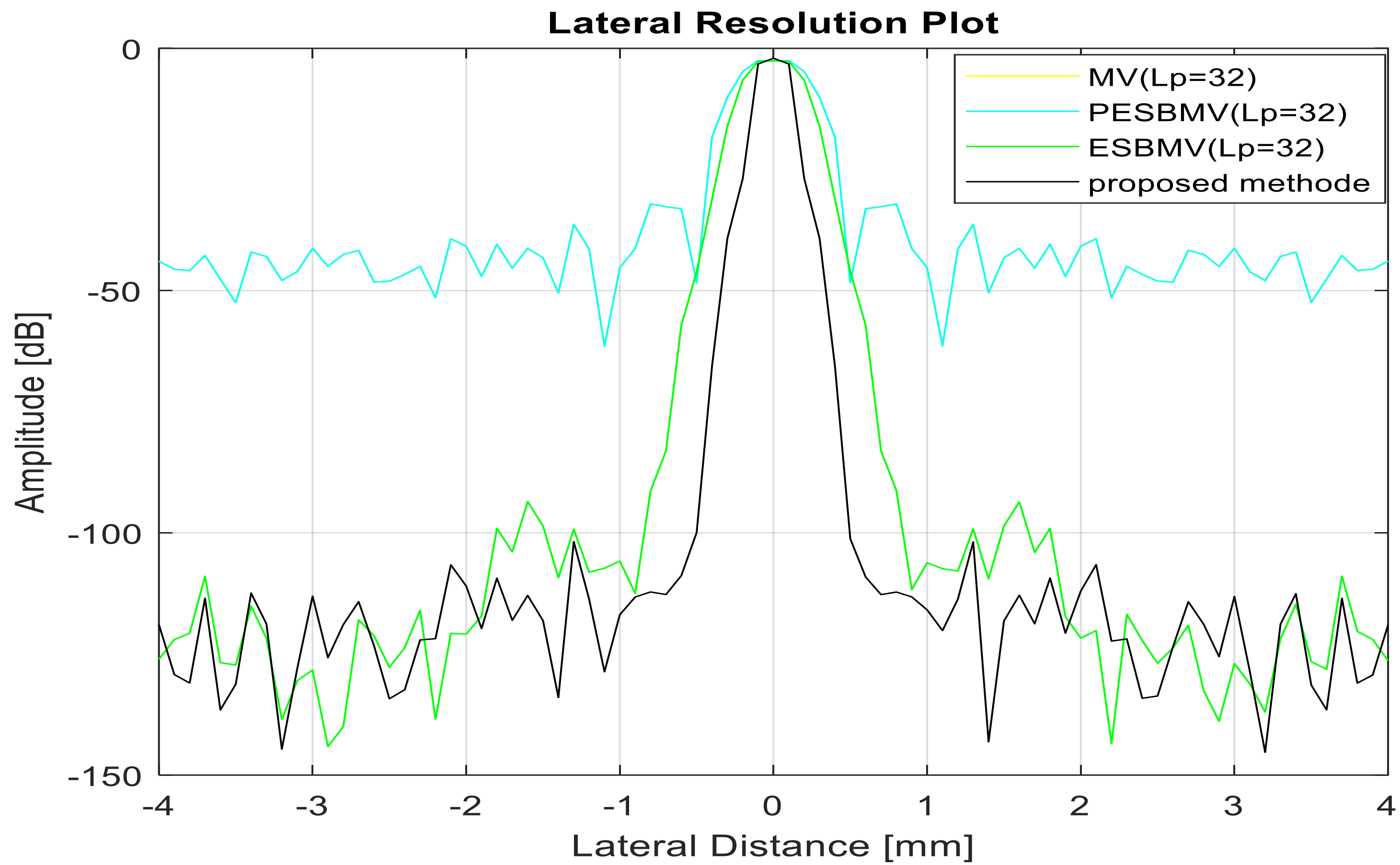

Figure (3.7): Comparing the lateral resolution profiles of the four simulated beamforming methods for the point located at 30.mm depth.

Table (3-1) Full Width at Half Maximum for the point located at the 30mm depth, for the beamformers shown in figure 3.6.

Method	FWHM (mm)
MV ($\boldsymbol{Lp = 32}$)	0.539
ESBMV ($\boldsymbol{Lp = 32}$)	0.441
PESBMV ((δ = 0.2, η = 0.5)	0.539
Proposed method (δ = 0.2, η = 0.5)	0.241

CHAPTER FOUR

IN VITRO DATASETS RESULTS

4.1 Introduction

This chapter is dedicated for evaluating the proposed method used in vitro datasets. In addition to B-mode images evaluating, the proposed method is evaluated and compared to other beamforming method using a number of ultrasound imaging quality metrics. These metrics include both contrast resolution and speckle SNR.

4.2 In Vitro Datasets

Two in vitro datasets are used in this dissertation to evaluate the proposed method. The datasets are obtained from the web platform of the International Ultrasound Symposium IEEE 2016 held in Tours, France [80]. A Verasonics Vantage 256 research scanner and an L11 probe are used to collect data (Verasonics Inc., Redmond, WA). CIRS Multi-Purpose Ultrasound Phantom (Model 040GSE) is used to collect those datasets for the modules shown in (a) for both figure 3.1 and figure 3.2 [81]. The first dataset for the module in figure 3.1(a) has three anechoic cysts and a single point target. They are embedded in background speckles. During this chapter, this dataset will be called (contrast dataset), due to including hypoechoic targets, allowing for doing contrast measurements.

The second dataset is shown in figure 3.2 (a). It includes a single hyperechoic lesion and seven point targets, embedded in background speckles [82]. This dataset will be called (resolution dataset) during this dissertation, due to including several point targets allowing for doing measurements of resolution at various imaging depths. MATLAB program is used to implement the proposed method as well as MV, ESBMV, and PESBMV methods for assessment and compression.

A linear array is used, consisting of 128 elements, each element has a width of 0.27 mm, a height of 6.0 mm, and a pitch of 0.3 mm. 6 MHz central frequency, 100% bandwidth, and 20.832 MHz sampling frequency are used. All the 128 elements were used during the transmission and reception, with a dynamic focus on the receiver and no focusing at the transmitter. The excitation sinusoidal wave has a pulse duration of 2.5 cycles. It is assumed that the medium sound speed is 1540m/s.

4.3 Results

In this dissertation, a variety of beamformers are applied to the in vitro datasets to be compared with the proposed beamformer's performance. Figure 4.6 displays the superiority of the proposed method in improving CR. Where, as shown in (a) and (b) in figure 4.1, MV $(Lp = 1)$ and MV $(Lp = M/2)$ produce blurred boundaries for the hypoechoic cyst targets.

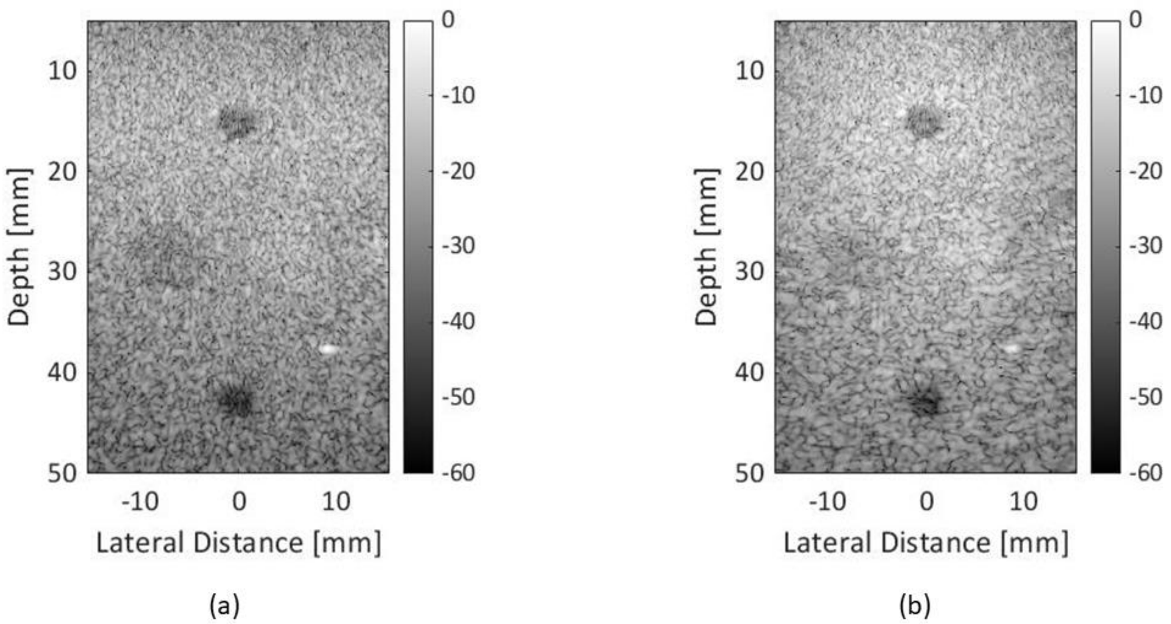

Figure (4.1): Images of in vitro data of the contrast dataset using: (a) MV $(Lp = 1)$ (b) MV $(Lp = M/2)$.

While there is noticeable distortion in background homogeneity due to the produced artifacts in ESBMV ($Lp = M/4, M/2$), as shown in figure 4.2 and 4.3. Figure (4.2): Images of the contrast dataset using: (a) ESBMV ($Lp = M/4$) (b) ESBMV ($Lp = M/2$)

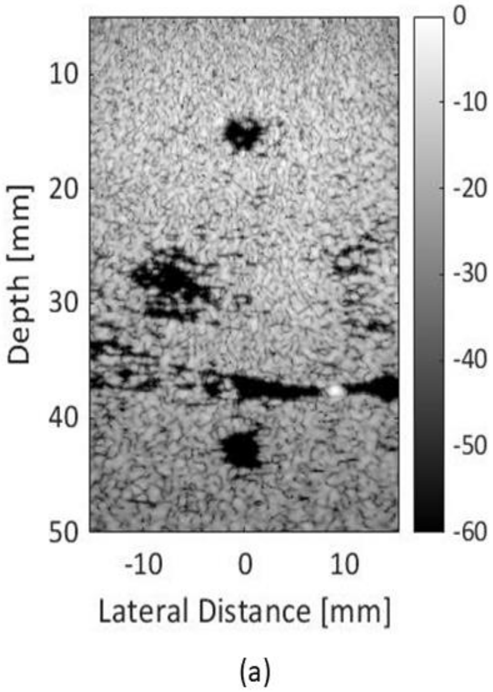

Figure (4.3): Images of in vitro data of the contrast dataset using: (a) ESBMV ($Lp = M/4$) (b) ESBMV ($Lp = M/2$)

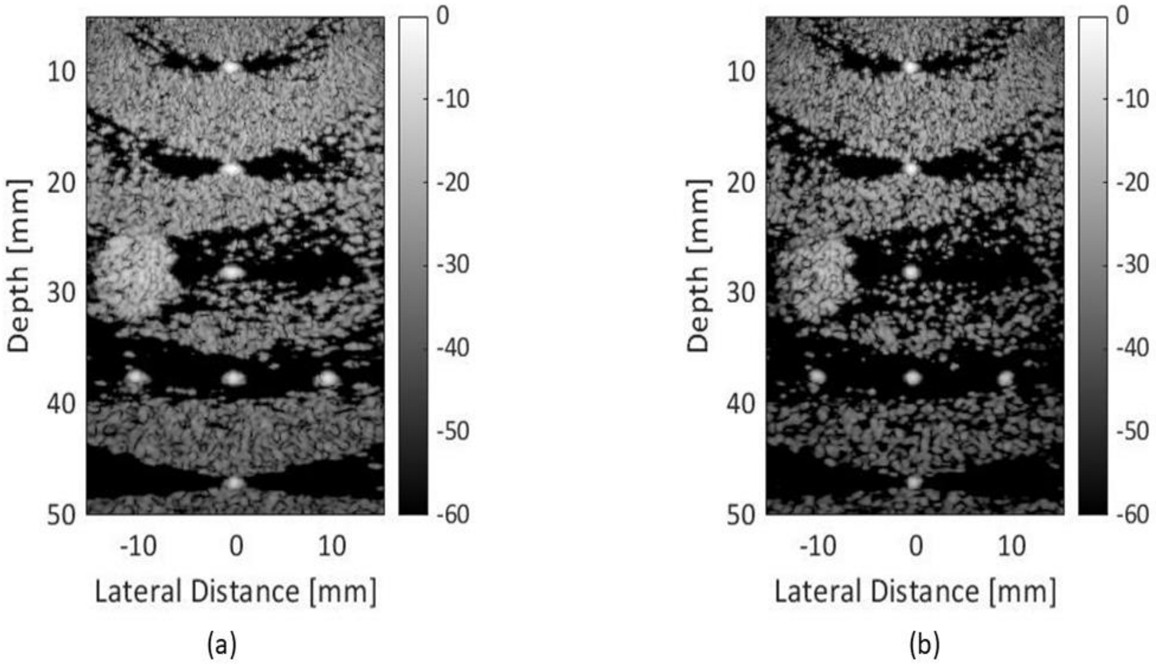

Figure (4.4): Images of in vitro data of the resolution dataset using: (a) ESBMV ($Lp = M/4$) (b) ESBMV ($Lp = M/2$).

ESBMV ($Lp = M/4$) and PESBMV ($Lp = M/4$) have a reduced CR compared to ESBMV ($Lp = M/2$) as can be seen in table 4.1.

The speckle pattern produced by MV ($Lp = M/2$) is homogeneous, while in ESBMV method, the background speckle suffers from strong BBRs. PESBMV method is better than ESBMV in limiting dark spots and BBR. Nevertheless, the background speckle using MV ($Lp = 1$ and $M/2$) as in figure 4.1 is still superior. This is comparable to DAS beamforming technique, which is known to give a highly homogeneous background.

Table 4.1 indicates that SSNR for the proposed method and MV with ($Lp = 1$) are close, which illustrates the strength of the proposed method in preserving the homogeny of speckle background.

Lateral responses of the implemented beamformers for the point target positioned at the 18.75 mm depth in the resolution phantom dataset are given in figure 4.7 to aid intuitive observations of their lateral resolution performance. The graphs show that when Lp increases, both of MV and ESBMV methods considerably result in reducing mainlobe width, where, compared to the other approaches, MV ($LP = 1$) is less effective in improving lateral resolution since its mainlobe width is theoretically equivalent to that of DAS. Lateral resolution in PESBMV approaches that in ESBMV method using the same subarray length (Lp), from table 4.2, it can be noticed that the smallest value of FWHM has been achieved using the proposed method, with an improvement by (52%) compared to the resolution achieved using PESBMV as shown in figure 4.4. One exception is FWHM in ESBMV at $Lp = M/4$, which produces very strong BBR artifacts as can be noticed from table 4.2 (the values of $SSNR_{\mathrm{BBR}}$) and in figures 4.5 and 4.6.

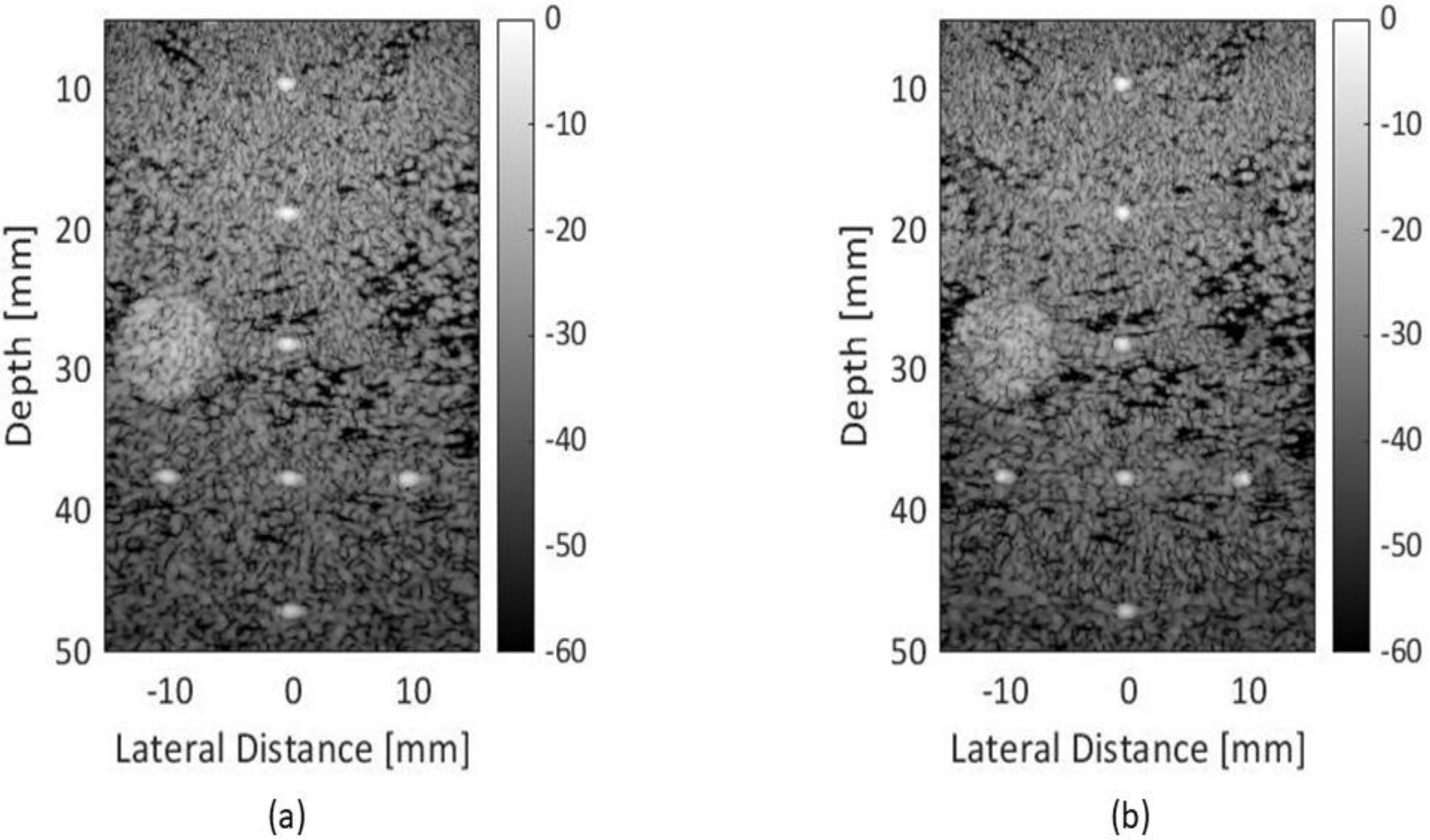

Figure (4.5) : Images of in vitro data of the resolution dataset using (a) PESBMV (δ = 0.2, η = 0.5, $Lp = M/4$) (b) proposed method (δ = 0.2, η = 0.5).

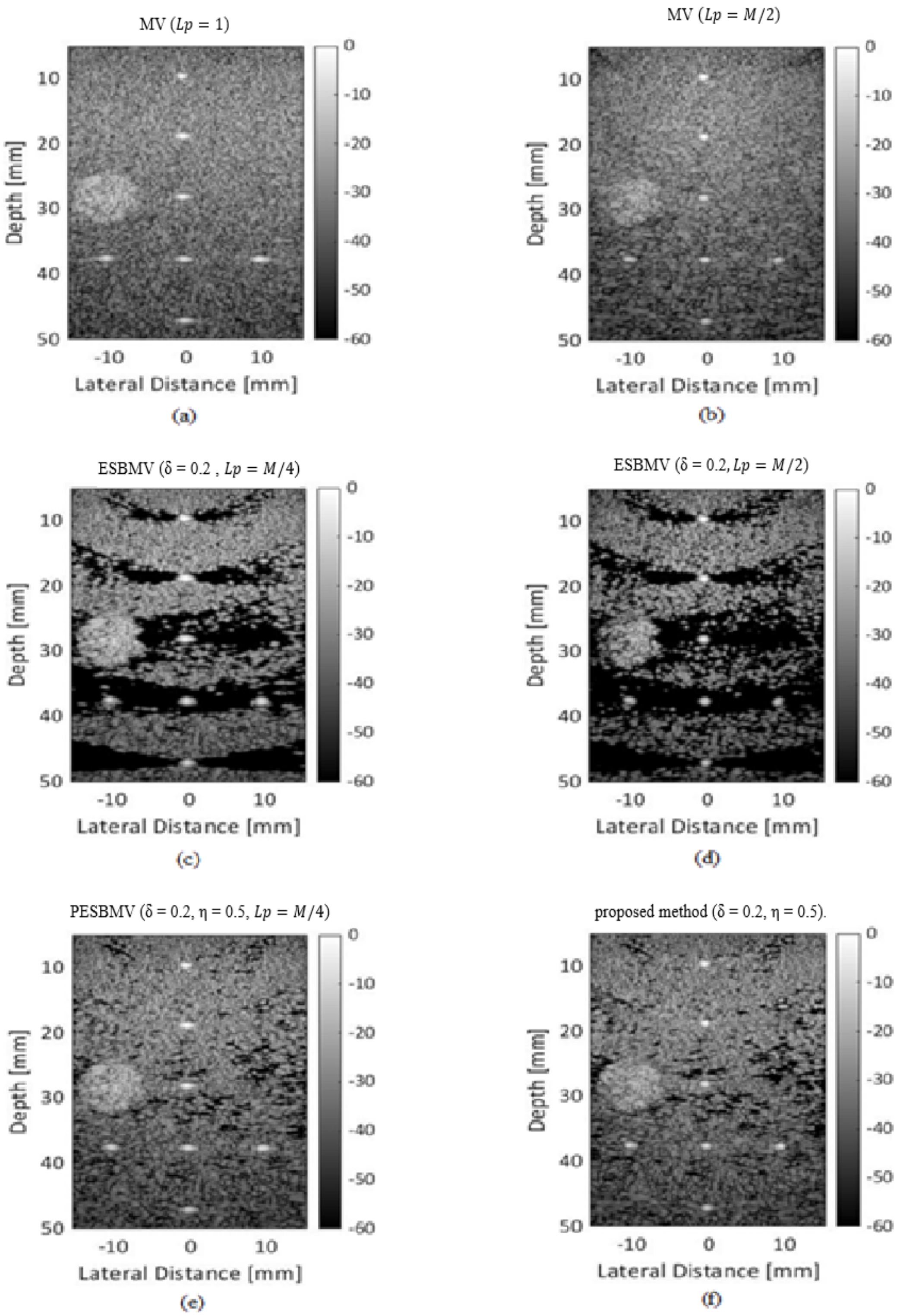

Figure (4.6): Images of in vitro data of the resolution dataset using different beamforming method. All images are shown in a dynamic range of 60 dB.

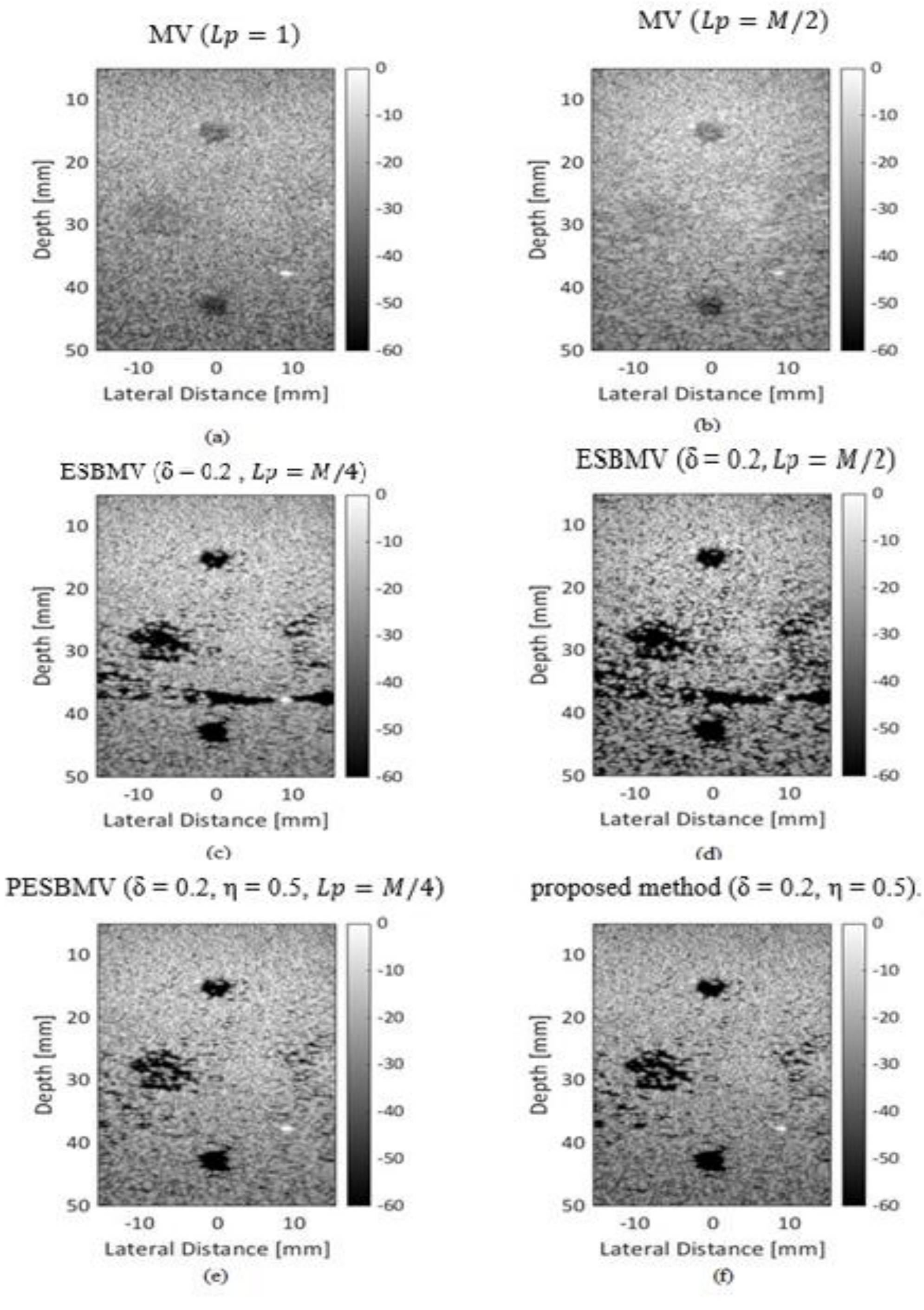

Figure (4.7): Images of in vitro data of contrast dataset using different beamforming method. All images are shown in a dynamic range of 60dB.

Table (4-1): Measurement of contrast and speckle statistics for the contrast dataset using different beamforming techniques.

Method	CR (dB)	CNR (dB)	SSNR
MV ($Lp = 1$)	12.36	2.05	1.74
MV ($Lp = M/2$)	11.85	1.97	1.65
ESBMV ($Lp = M/4$)	15.67	2.44	1.63
ESBMV ($Lp = M/2$)	17.17	2.12	1.30
PESBMV (δ=0.2, η=0.5)	15.57	2.42	1.63
Proposed method (δ=0.2, η=0.5)	16.26	2.55	1.70

Table (4-2): Measurements of SSNR at BBR and FWHM for the point target at 18.75 mm depth for the resolution phantom dataset using different beamforming techniques.

Method	FWHM (mm)	$SSNR_{BBR}$
MV ($Lp = 1$)	1.086	5.82
MV ($Lp = M/2$)	0.709	6.33
ESBMV ($Lp = M /4$)	0.978	2.29
ESBMV ($Lp = M /2$)	0.648	2.56
PESBMV ((δ = 0.2, η = 0.5)	0.987	6.03
Proposed method (δ = 0.2, η = 0.5)	0.704	5.89

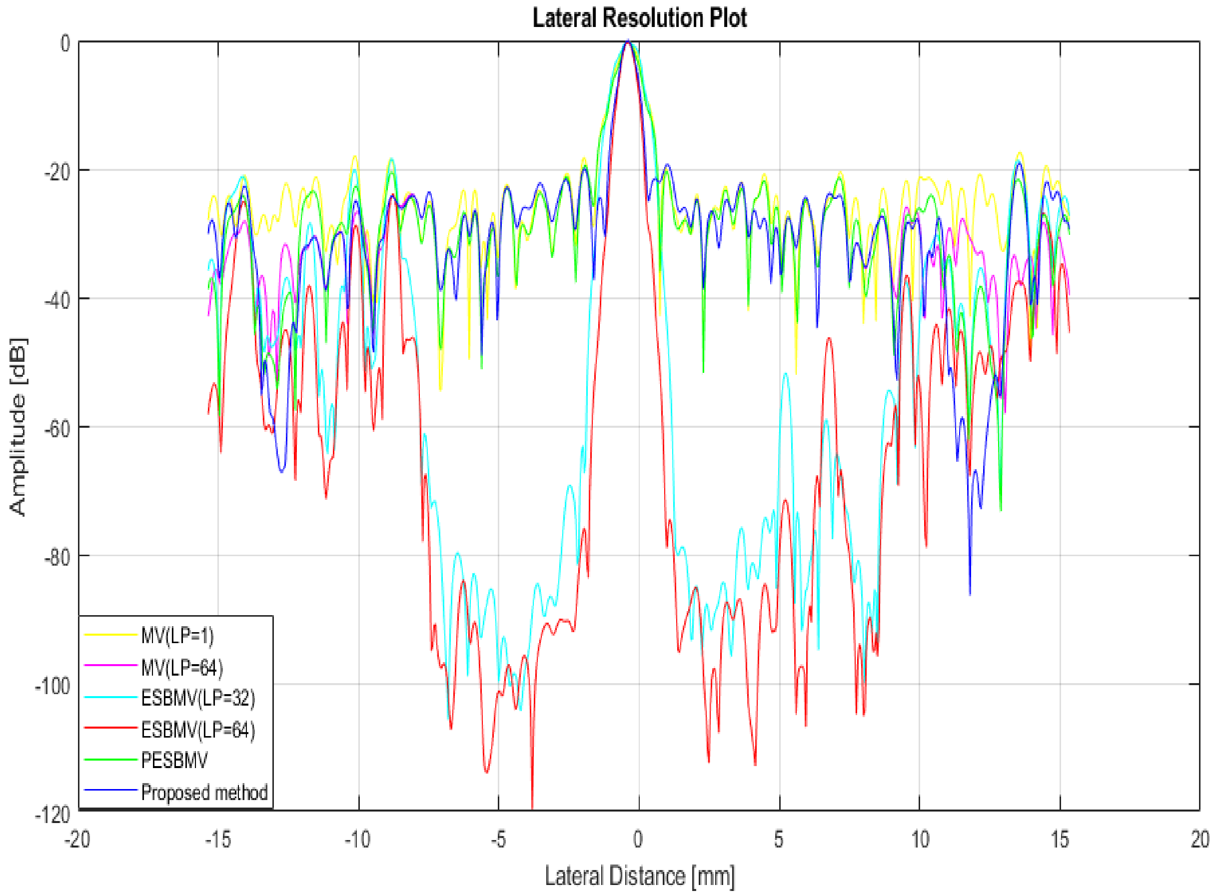

Figure (4.8): Lateral profiles displayed for the point target located at the 18.75 mm depth for the resolution phantom.

4.4 Analysis of Results

The proposed algorithm proves to be highly effective in increasing the quality of imaging through improving image contrast and preserving speckle pattern. It also proves to be significantly increasing lateral resolution. This is done by sensing the details of the image first through the value of Num, which can efficiently distinguish hyperechoic targets and sidelobe regions from the rest of the regions, as it gives a value (1) for the hyperechoic target and a value between 2 and half subarray length to sidelobe regions as can be noticed from (b) in figure 3.1 and figure 3.2. Secondly by using the value of the weights of ESBMV ($Lp = M/4$). This is because the values of this weight given to the cyst are found to be within the range from 0 to 0.5, as can be noticed from (c) in figure 3.1 and figure 3.2.

Figure 4.6 illustrates that the cyst is much more visible using the proposed method and that the proposed beamformer significantly improves CNR, exceeding all the implemented beamforming methods.

The main reason for that is the ability of the proposed method to detect the areas of the cysts, and because of the use of the CF that justifies the weight of the beamformer based on the coherency of these signals and due to the projection of the MV weights onto the signal subspace. Also, to improve speckle statistics and contrast in tissue areas, temporal smoothing is applied, where the final value of the focal point is determined by a vector of samples instead of a single sample.

The proposed method's superiority in terms of CR and CNR is confirmed through the results of table 4.1. When the weight of ESBMV($Lp = M/4$) is higher than (0.5), this indicates being inside the areas of the speckle. The proposed method uses MV ($Lp = 1$) in this region to produce more homogenous background speckle and thus higher values of SSNR are achievable.

The issue of the underestimation of the amplitude of hyperechoic targets when a large length of the subarray is used has been solved by surrounding the hyperechoic and wire areas by MV ($\mathrm{Lp} = \mathrm{M}/2$), while beamforming inside the regions of the hyperechoic and wire targets using MV ($\mathrm{Lp} = 1$). The results of using this method are described in tables 4.1 and 4.2.

4.5 Unsuccessful Examined Methods

This part discusses a set of methods that have been examined for discriminating image regions before reaching the final algorithm proposed in this dissertation. Those implemented methods were not considered due to either providing unsignificant improvement to the final image or because they were unable to distinguish image parts from one another. Those factors include Coherence Factor (CF), coherent sum, standard deviation, and Wiener postfilter.

4.5.1 Coherent Summation of Received Signals

Coherent sum means to coherently add the values of x(k) for each focal point. It also represents the numerator in the equation of CF. It was suggested to be examined for discrimination due to having the ability to highly discriminate between hypoechoic targets which have highly coherent signals, and speckle background which include incoherent signals. For the same reason, coherent summation is expected to be able to discriminate hyperechoic targets from sidelobe regions. Figure 4.8 shows the result of coherent summation of contrast dataset.

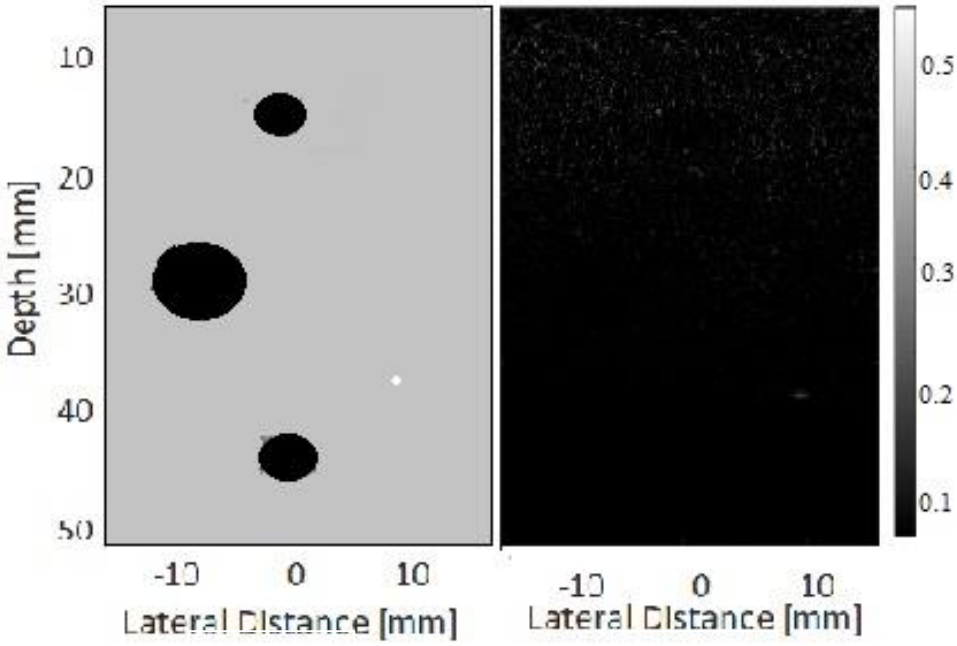

(a) (b)

Figure (4.9): (b)The result of coherent summation of the contrast phantom shown in (a).

However, the result of coherently summing received data, as shown in figure 4.b, has failed to distinguish between hypoechoic targets and background. This is because this summation is not a ratio and therefore it becomes lower as depth increases and therefore the use of coherence factor (CF) was suggested to solve this problem.

4.5.2 Coherence Factor

One of the examined methods for discrimination is the coherence factor explained in section (2.16). This factor was proposed due to having the ability to highly discriminate between hyperechoic targets and sidelobe regions, while it is expected not to make a good discrimination in the other region containing hypoechoic targets and background speckle, due to its inability to retain homogeneity and producing dark spots in background speckle, which makes it hard to discriminate many points in this area from cysts. Figure (4.9) shows the value of CF using contrast phantom.

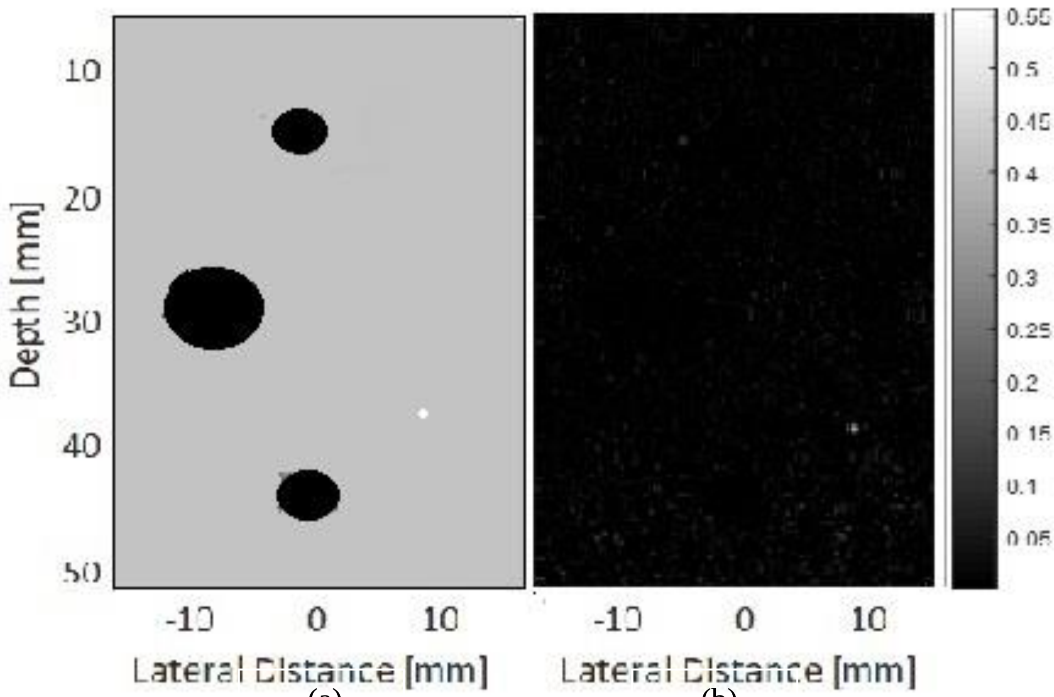

(a) (b)

Figure (4.10):(b) The result of the coherence factor of the contrast phantom shown in (a).

As expected, figure 4.9 shows that CF highly distorts background homogeneity and thus fails to be suitable for distinguishing in the first region (hypoechoic targets and background). In the second region (containing hyperechoic targets and sidelobes), CF was efficiently able to discriminate between regions. This means that it could be used as a discrimination tool in this area. However, it was not considered for this job, and this is because the use of Num was able to give an even better results and the latter is therefore considered as a discrimination tool in this region in the proposed method.

4.5.3 Standard Deviation

In statistics, the standard deviation is a measure of the amount of variation or dispersion of a set of values. It tells how spread out from the center of the distribution the data is on average. A low standard deviation indicates that the values tend to be close to the mean of the set, while a high standard deviation indicates the opposite.

Due to the mentioned properties of standard deviation, it was suggested for distinguishing image regions, where standard deviations are calculated for the signal subspace matrix of ESBMV. Figure 4.10 shows these values of σ using the contrast phantom.

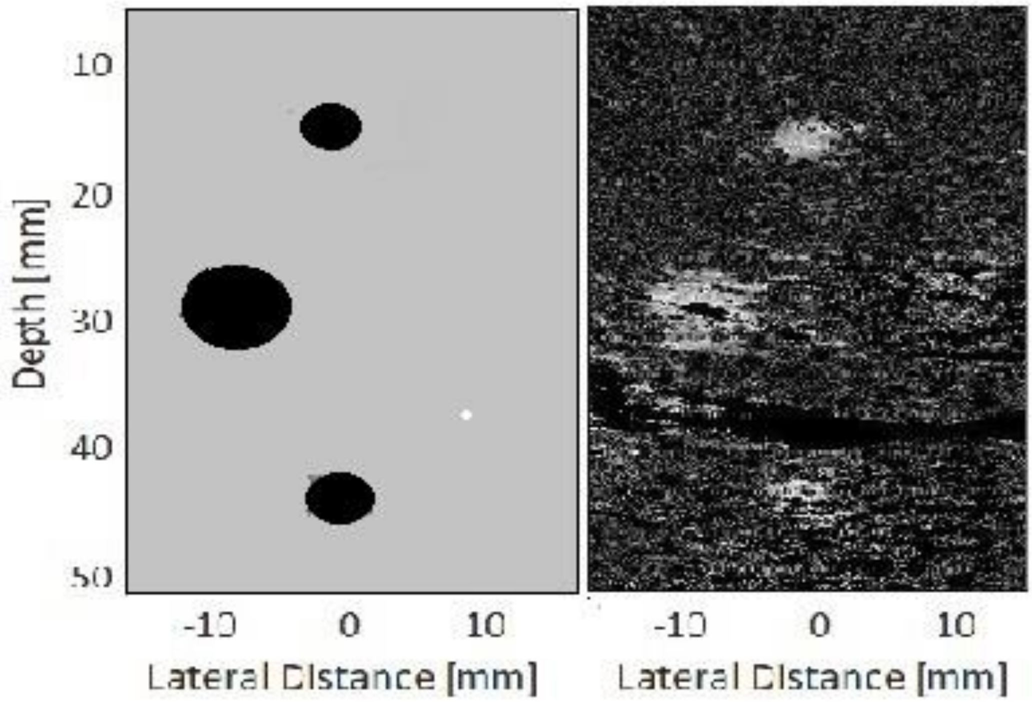

(a) (b)

Figure (4.11): (b) The results of the value of standard deviation of the contrast phantom shown (a).

From figure 4.10 it can be seen that σ was not able to discriminate between wires and sidelobes, while it was able to discriminate between cysts and backgrounds but with lower performance than the proposed method.

4.5.4 Wiener Post Filter

The Wiener filter, also known as the Wiener post-filter, as explained in section (2.17), is tested for discriminating image regions. Figure 4.11 shows the output values of wiener postfiltering applied to the contrast phantom.

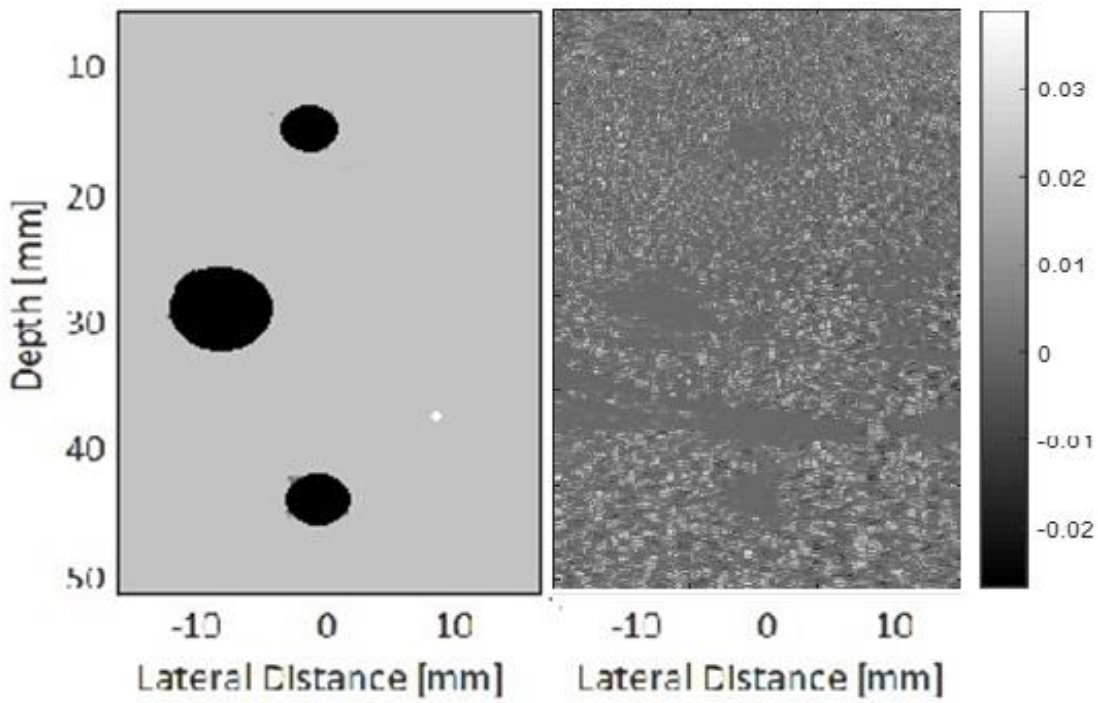

(a) (b)

Figure (4.12): (b) The results of wiener filter applied to the contrast phantom shown in (a).

From figure 4.11 it can be seen that Wiener post filter fails as a discriminating tool in the region containing cysts and speckle background, because of the highly distorting speckle and producing dark spots, in addition to providing widened and distorted wire target in the region containing hyperechoic targets and sidelobes, which makes Wiener post filter unsuitable for this task.

CHAPTER FIVE

CONCLUSIONS AND FUTURE WORK

5.1 Conclusions

The technique of transforming received echo signals into a picture to characterize the region of interest is known as beamforming. This dissertation focuses on Plane-Wave Imaging (PWI) beamformers, which create a complete ultrasound image for the area of interest with a single transmission. This enables data acquisition at rates greater than 1000 frames per second, enabling for new ultrafast imaging applications such as shear wave tracking and flow motion estimates. Meanwhile, other beamforming techniques have been developed to compensate for PWI's lack of focusing, which reduces imaging quality. This dissertation deals with different types of beamformers.

For PESBMV, it is concluded that PESBMV is a good method suggested to eliminate BBR artifacts appear in reference ESBMV, but with decreasing the contrast ratio as a drawback. This dissertation introduces a novel approach for improving image quality produced by PESBMV. The new algorithm which discriminates imaging area based on Num and the weight of ESBMV is meant to improve lateral resolution and speckle preservation while simultaneously increasing contrast by using different beamforming types in each defined area. The results show that the proposed approach can achieve increased image contrast and very well keep speckle patterns with a significant increase in lateral resolution. Most importantly, it can keep BBRs, and dark spots minimized. Additionally, the proposed approach has the potential to be an effective strategy for improving image quality in other imaging methods such as Compound Plane Wave Imaging (CPWI).

5.2 Future work

The current work can be extended by performing the following:

1. Combining the proposed algorithm with other types of beamforming methods such as CPWI. This is because merging beamformers with this method usually results in further improvement in imaging quality.
2. Merging the proposed method with (Salaris method) which suggests to adaptively generating the parameters that control MV performance balance so that this beamformer is fully independent on the user.
3. Using Wiener post filtering with proposed method in specific region.

REFERENCES

[1] J. Li, J. Chen, Y. Tang, C. Wang, B. A. Landman, and S. K. Zhou, "Transforming medical imaging with Transformers? A comparative review of key properties, current progresses, and future perspectives," *Med Image Anal*, p. 102762, 2023.

[2] J. Vassileva and O. Holmberg, "Radiation protection perspective to recurrent medical imaging: what is known and what more is needed?," *Br J Radiol*, vol. 94, no. 1126, p. 20210477, 2021.

[3] V. Chan and A. Perlas, "Basics of ultrasound imaging," in *Atlas of Ultrasound-Guided Procedures in Interventional Pain Management*, Springer, 2011, pp. 13–19. doi: 10.1007/978-1-4419-1681-5_2.

[4] C. M. Otto, "Principles of echocardiographic image acquisition and Doppler analysis," *Otto CM: Textbook of clinical echocardiography. WB Saunders, Philadelphia*, pp. 1–3, 2000.

[5] "Different Uses for Ultrasound - Medical Associates of Northwest Arkansas." Accessed: Aug. 09, 2023. [Online]. Available: https://www.mana.md/different-uses-for-ultrasound/

[6] S.-J. Shin and B.-J. Jeong, "Principle and comprehension of ultrasound imaging," *Journal of the Korean Orthopaedic Association*, vol. 48, no. 5, pp. 325–333, 2013.

[7] A. E. Weyman, *Principles and practice of echocardiography*. Lea & Febiger, 1994.

[8] H. Kuttruff and H. Kuttruff, "Generation and Detection of Sound with Frequencies Above 1 GHz (Hypersound)," *Ultrasonics: Fundamentals and Applications*, pp. 187–205, 1991.

[9] T. Szasz, "Advanced beamforming techniques in ultrasound imaging and the associated inverse problems," *Medical Imaging. Université Toulouse*, vol. 3, 2016.

[10] O. Villemain *et al.*, “Ultrafast ultrasound imaging in pediatric and adult cardiology: techniques, applications, and perspectives,” *Cardiovascular Imaging*, vol. 13, no. 8, pp. 1771–1791, 2020.

[11] W. Wang, Q. He, Z. Zhang, and Z. Feng, “Adaptive beamforming based on minimum variance (ABF-MV) using deep neural network for ultrafast ultrasound imaging,” *Ultrasonics*, vol. 126, p. 106823, 2022.

[12] C.-C. Lee and J.-H. Lee, “Eigenspace-based adaptive array beamforming with robust capabilities,” *IEEE Trans Antennas Propag*, vol. 45, no. 12, pp. 1711–1716, 1997.

[13] S. Mehdizadeh, A. Austeng, T. F. Johansen, and S. Holm, “Eigenspace based minimum variance beamforming applied to ultrasound imaging of acoustically hard tissues,” *IEEE Trans Med Imaging*, vol. 31, no. 10, pp. 1912–1921, 2012.

[14] B. D. Van Veen, “Eigenstructure based partially adaptive array design,” *IEEE Trans Antennas Propag*, vol. 36, no. 3, pp. 357–362, 1988.

[15] B. M. Asl and A. Mahloojifar, “Eigenspace-based minimum variance beamforming applied to medical ultrasound imaging,” *IEEE Trans Ultrason Ferroelectr Freq Control*, vol. 57, no. 11, pp. 2381–2390, 2010.

[16] X. Zeng, C. Chen, and Y. Wang, “Eigenspace-based minimum variance beamformer combined with Wiener postfilter for medical ultrasound imaging,” *Ultrasonics*, vol. 52, no. 8, pp. 996–1004, 2012.

[17] X. Zeng, Y. Wang, J. Yu, and Y. Guo, “Correspondence-beam-domain eigenspace-based minimum variance beamformer for medical ultrasound imaging,” *IEEE Trans Ultrason Ferroelectr Freq Control*, vol. 60, no. 12, pp. 2670–2676, 2013.

[18] S. Aliabadi, J. Yu, and Y. Wang, “Enhance contrast in PCA based beamformers using smoothing kernel,” *Biomed Mater Eng*, vol. 26, no. s1, pp. S1613–S1621, 2015.

[19] J. Zhao, Y. Wang, J. Yu, W. Guo, T. Li, and Y.-P. Zheng, "Subarray coherence based postfilter for eigenspace based minimum variance beamformer in ultrasound plane-wave imaging," *Ultrasonics*, vol. 65, pp. 23–33, 2016.

[20] Z. Rami Alomari, "Plane Wave Imaging Beamforming Techniques for Medical Ultrasound Imaging*," PhD Thesis. University of Leeds.* 2017.

[21] X. Wu, Q. Gao, M. Lu, T. Wang, and S. Chen, "An improved spatio-temporally smoothed coherence factor combined with eigenspace-based minimun variance beamformer for plane-wave imaging in medical ultrasound," in *2017 IEEE International Ultrasonics Symposium (IUS)*, IEEE, 2017, pp. 1–4.

[22] Y. Wang, C. Zheng, H. Peng, and X. Chen, "Short-lag spatial coherence combined with eigenspace-based minimum variance beamformer for synthetic aperture ultrasound imaging," *Comput Biol Med*, vol. 91, pp. 267–276, 2017.

[23] M. Mozaffarzadeh, S. A. O. I. Avanji, A. Mahlooiifar, and M. Orooji, "Photoacoustic imaging using combination of eigenspace-based minimum variance and delay-multiply-and-sum beamformers: Simulation study," in *2017 24th National and 2nd International Iranian Conference on Biomedical Engineering (ICBME)*, IEEE, 2017, pp. 1–5.

[24] M. Mozaffarzadeh, A. Mahloojifar, V. Periyasamy, M. Pramanik, and M. Orooji, "Eigenspace-based minimum variance combined with delay multiply and sum beamformer: Application to linear-array photoacoustic imaging," *IEEE Journal of Selected Topics in Quantum Electronics*, vol. 25, no. 1, pp. 1–8, 2018.

[25] S. Shamekhi, V. Periyasamy, M. Pramanik, M. Mehrmohammadi, and B. M. Asl, "Eigenspace-based minimum variance beamformer combined with sign coherence factor: Application to linear-array photoacoustic imaging," *Ultrasonics*, vol. 108, p. 106174, 2020.

[26] Z. Lan, C. Zheng, Y. Wang, H. Peng, and H. Qiao, “Adaptive threshold for eigenspace-based minimum variance beamformer for dark region artifacts elimination,” *IEEE Trans Instrum Meas*, vol. 70, pp. 1–16, 2021.

[27] R. S. C. Cobbold, *Foundations of biomedical ultrasound*. Oxford university press, 2006.

[28] C. Deane, “Ultrasonography in Vascular Diagnosis. A Therapy-Oriented Textbook and Atlas,” *Ultrasound Med Biol*, vol. 38, no. 2, p. 346, 2012.

[29] J. Bercoff, “Ultrafast ultrasound imaging,” *Ultrasound imaging-Medical applications*, pp. 3–24, 2011.

[30] Franco, Alessandro, and Carlo Bartoli. "The ultrasounds as a mean for the enhancement of heat exchanger performances: an analysis of the available data." Journal of Physics: Conference Series. Vol. 1224. No. 1. IOP Publishing, 2019.

[31] M. Pernot and G. Goudot, “Noninvasive ultrafast ultrasound for imaging the coronary vasculature and assessing the arterial wall’s biomechanics,” in *Biomechanics of Coronary Atherosclerotic Plaque*, Elsevier, 2021, pp. 517–528.

[32] C. Jiang, C. Liu, Y. Zhan, and D. Ta, “The Spectrum-Beamformer for Conventional B-Mode Ultrasound Imaging System: Principle, Validation, and Robustness,” *Ultrason Imaging*, vol. 44, no. 2–3, pp. 59–76, 2022.

[33] P. Gallego and I. Valverde, *Multimodality imaging innovations in adult congenital heart disease*. Springer, 2021.

[34] “kidney in ultrasound b mode scan - Bing images.” Accessed: Dec. 12, 2023. [Online].Available:https://www.bing.com/images/search?view=detailV2&ccid=eFF54om7&id=F8AD4F1F7919530867AE4B06F24279EE690B820B&thid=OIP.eFF54om7WRqZCAxbIstCoAHaFj&mediaurl=https%3a%2f%2fwww.medison.ru%2fultrasound%2fimg%2fb687.jpg&cdnurl=https%3a%2f%2fth.bing.com%2fth%2fid%2fR.785179e289bb591a99080c5b22cb42a0%3frik

%3dC4ILae55QvIGSw%26pid%3dImgRaw%26r%3d0&exph=600&expw=800&q=kidney+in+ultrasound+b+mode+scan+-+Bing+images&simid=608048227422203086&FORM=IRPRST&ck=4E8A27AAAE40DE52CE5ED784C3B9983F&selectedIndex=0&itb=0&idpp=overlayview&ajaxhist=0&ajaxserp=0.

[35] N. T. Schiefler Jr, J. M. Maia, F. K. Schneider, A. J. Zimbico, A. A. Assef, and E. T. Costa, "Generation and analysis of ultrasound images using plane wave and sparse arrays techniques," *Sensors*, vol. 18, no. 11, p. 3660, 2018.

[36] J. Foiret, X. Cai, H. Bendjador, E.-Y. Park, A. Kamaya, and K. W. Ferrara, "Improving plane wave ultrasound imaging through real-time beamformation across multiple arrays," *Sci Rep*, vol. 12, no. 1, p. 13386, 2022.

[37] "Using Ultrasound Plane Wave Imaging in NDT | Zetec." Accessed: Apr. 29, 2023. [Online]. Available: https://www.zetec.com/blog/ultrasound-plane-wave-imaging-ndt/

[38] H. Hasegawa and C. L. De Korte, "Special issue on ultrafast ultrasound imaging and its applications," *Applied Sciences*, vol. 8, no. 7. MDPI, p. 1110, 2018.

[39] D. Maresca *et al.*, "Noninvasive imaging of the coronary vasculature using ultrafast ultrasound," *JACC Cardiovasc Imaging*, vol. 11, no. 6, pp. 798–808, 2018.

[40] P. Santos *et al.*, "Natural shear wave imaging in the human heart: normal values, feasibility, and reproducibility," *IEEE Trans Ultrason Ferroelectr Freq Control*, vol. 66, no. 3, pp. 442–452, 2018.

[41] J. Grondin, D. Wang, C. S. Grubb, N. Trayanova, and E. E. Konofagou, "4D cardiac electromechanical activation imaging," *Comput Biol Med*, vol. 113, p. 103382, 2019.

[42] M. Correia, T. Deffieux, S. Chatelin, J. Provost, M. Tanter, and M. Pernot, "3D elastic tensor imaging in weakly transversely isotropic soft tissues," *Phys Med Biol*, vol. 63, no. 15, p. 155005, 2018.

[43] A. Costet *et al.*, "Non-invasive characterization of focal arrhythmia with electromechanical wave imaging in vivo," *Ultrasound Med Biol*, vol. 44, no. 11, pp. 2241–2249, 2018.

[44] M. Tanter and M. Fink, "Ultrafast imaging in biomedical ultrasound," *IEEE Trans Ultrason Ferroelectr Freq Control*, vol. 61, no. 1, pp. 102–119, 2014.

[45] O. Villemain *et al.*, "Ultrafast ultrasound imaging in pediatric and adult cardiology: techniques, applications, and perspectives," *Cardiovascular Imaging*, vol. 13, no. 8, pp. 1771–1791, 2020.

[46] R. E. McKeighen and M. P. Buchin, "New techniques for dynamically variable electronic delays for real time ultrasonic imaging," in *1977 Ultrasonics Symposium*, IEEE, 1977, pp. 250–254.

[47] V. Perrot, M. Polichetti, F. Varray, and D. Garcia, "So you think you can DAS? A viewpoint on delay-and-sum beamforming," *Ultrasonics*, vol. 111, p. 106309, 2021.

[48] R. J. Mailloux, "Phased array theory and technology," *Proceedings of the IEEE*, vol. 70, no. 3, pp. 246–291, 1982.

[49] F. Destrempes and G. Cloutier, "A critical review and uniformized representation of statistical distributions modeling the ultrasound echo envelope," *Ultrasound Med Biol*, vol. 36, no. 7, pp. 1037–1051, 2010.

[50] S. Salles, H. Liebgott, O. Basset, C. Cachard, D. Vray, and R. Lavarello, "Experimental evaluation of spectral-based quantitative ultrasound imaging using plane wave compounding," *IEEE Trans Ultrason Ferroelectr Freq Control*, vol. 61, no. 11, pp. 1824–1834, 2014.

[51] G. Montaldo, M. Tanter, J. Bercoff, N. Benech, and M. Fink, "Coherent plane-wave compounding for very high frame rate ultrasonography and

transient elastography," *IEEE Trans Ultrason Ferroelectr Freq Control*, vol. 56, no. 3, pp. 489–506, 2009.

[52] V. Madisetti, *Wireless, networking, radar, sensor array processing, and nonlinear signal processing*. CRC press, 2018.

[53] S. Afrakhteh and H. Behnam, "Low-complexity adaptive minimum variance ultrasound beam-former based on diagonalization," *Biomed Signal Process Control*, vol. 62, p. 102110, 2020.

[54] J.-F. Synnevag, A. Austeng, and S. Holm, "Benefits of minimum-variance beamforming in medical ultrasound imaging," *IEEE Trans Ultrason Ferroelectr Freq Control*, vol. 56, no. 9, pp. 1868–1879, 2009.

[55] J. Capon, "High-resolution frequency-wavenumber spectrum analysis," *Proceedings of the IEEE*, vol. 57, no. 8, pp. 1408–1418, 1969.

[56] Y. Wang, Y. Qi, and Y. Wang, "A low-complexity minimum-variance beamformer based on orthogonal decomposition of the compounded subspace," *Ultrason Imaging*, vol. 43, no. 1, pp. 3–18, 2021.

[57] M. Xu, Y. Chen, M. Ding, and Y. Ming, "Adaptive minimum variance beamforming combined with phase coherence imaging for ultrasound imaging," in *Medical Imaging 2012: Ultrasonic Imaging, Tomography, and Therapy*, SPIE, 2012, pp. 122–129.

[58] B. M. Asl and A. Mahloojifar, "Minimum variance beamforming combined with adaptive coherence weighting applied to medical ultrasound imaging," *IEEE Trans Ultrason Ferroelectr Freq Control*, vol. 56, no. 9, pp. 1923–1931, 2009.

[59] B. Luijten *et al.*, "Adaptive ultrasound beamforming using deep learning," *IEEE Trans Med Imaging*, vol. 39, no. 12, pp. 3967–3978, 2020.

[60] J. Li, G. Wei, and Y. Ding, "Adaptive beamforming based on covariance matrix reconstruction by exploiting interferences' cyclostationarity," *Signal Processing*, vol. 93, no. 9, pp. 2543–2547, 2013.

[61] Y. Gu, N. A. Goodman, S. Hong, and Y. Li, “Robust adaptive beamforming based on interference covariance matrix sparse reconstruction,” *Signal Processing*, vol. 96, pp. 375–381, 2014.

[62] R. Abrahamsson, Y. Selen, and P. Stoica, “Enhanced covariance matrix estimators in adaptive beamforming,” in *2007 IEEE International Conference on Acoustics, Speech and Signal Processing-ICASSP’07*, IEEE, 2007, pp. II–969.

[63] R. Zhuang and J. Chen, “High Contrast Minimum Variance Beamforming Combined with Convolutional Neural Network,” in *2019 IEEE International Ultrasonics Symposium (IUS)*, IEEE, 2019, pp. 564–567.

[64] X. Yan and Y. Wang, “A submatrix spatial coherence approach to minimum variance beamforming combined with sign coherence factor for coherent plane wave compounding,” *Technology and Health Care*, no. Preprint, pp. 1–15, 2022.

[65] A. Salari and B. M. Asl, “User parameter-free minimum variance beamformer in medical ultrasound imaging,” *IEEE Trans Ultrason Ferroelectr Freq Control*, vol. 68, no. 7, pp. 2397–2406, 2021.

[66] I. K. Holfort, F. Gran, and J. A. Jensen, “Broadband minimum variance beamforming for ultrasound imaging,” *IEEE Trans Ultrason Ferroelectr Freq Control*, vol. 56, no. 2, pp. 314–325, 2009.

[67] M. Sasso and C. Cohen-Bacrie, “Medical ultrasound imaging using the fully adaptive beamformer,” in *Proceedings.(ICASSP’05). IEEE International Conference on Acoustics, Speech, and Signal Processing, 2005.*, IEEE, 2005, pp. ii–489.

[68] J. F. Synnevag, A. Austeng, and S. Holm, “Adaptive beamforming applied to medical ultrasound imaging,” *IEEE Trans Ultrason Ferroelectr Freq Control*, vol. 54, no. 8, pp. 1606–1613, 2007.

[69] T.-J. Shan and T. Kailath, “Adaptive beamforming for coherent signals and interference,” *IEEE Trans Acoust*, vol. 33, no. 3, pp. 527–536, 1985.

[70] J.-F. Synnevåg, C.-I. Nilsen, and S. Holm, “P2b-13 speckle statistics in adaptive beamforming,” in *2007 IEEE Ultrasonics Symposium Proceedings*, IEEE, 2007, pp. 1545–1548.

[71] Y. Wang, Y. Wang, M. Liu, Z. Lan, C. Zheng, and H. Peng, “Minimum variance beamforming combined with covariance matrix-based adaptive weighting for medical ultrasound imaging,” *Biomed Eng Online*, vol. 21, no. 1, p. 40, 2022.

[72] X. Li, P. Wang, and Q. Li, “Frequency Domain Eigenspace-based Projection Minimum Variance for Ultrasound Imaging,” in *2022 IEEE Signal Processing in Medicine and Biology Symposium (SPMB)*, IEEE, 2022, pp. 1–4.

[73] K. W. Hollman, K. W. Rigby, and M. O’donnell, “Coherence factor of speckle from a multi-row probe,” in *1999 IEEE Ultrasonics Symposium. Proceedings. International Symposium (Cat. No. 99CH37027)*, IEEE, 1999, pp. 1257–1260.

[74] S. A. I. Avanji, A. M. Far, and B. M. Asl, “Investigation of the effects of transducer Parameters on adaptive MV beamformers in medical ultrasound applications,” in *2013 21st Iranian Conference on Electrical Engineering (ICEE)*, IEEE, 2013, pp. 1–6.

[75] C.-I. C. Nilsen and S. Holm, “Wiener beamforming and the coherence factor in ultrasound imaging,” *IEEE Trans Ultrason Ferroelectr Freq Control*, vol. 57, no. 6, pp. 1329–1346, 2010.

[76] M. Hisatsu, S. Mori, M. Arakawa, and H. Kanai, “Application of low-complexity generalized coherence factor to in vivo data,” *Journal of Medical Ultrasonics*, vol. 49, no. 4, pp. 555–567, 2022.

[77] N. E. Bylund, M. Ressner, and H. Knutsson, “3D wiener filtering to reduce reverberations in ultrasound image sequences,” in *Image Analysis: 13th Scandinavian Conference, SCIA 2003 Halmstad, Sweden, June 29–July 2, 2003 Proceedings 13*, Springer, 2003, pp. 579–586.

[78] “Field II Ultrasound Simulation Program.” Accessed: Aug. 20, 2023. [Online]. Available: https://www.field-ii.dk/

[79] S. Harput, J. McLaughlan, D. M. J. Cowell, and S. Freear, “New performance metrics for ultrasound pulse compression systems,” in *2014 IEEE International Ultrasonics Symposium*, IEEE, 2014, pp. 440–443.

[80] “WELCOME TO IEEE IUS 2016 - 2016 IEEE International Ultrasonics Symposium.” Accessed: Apr. 16, 2023. [Online]. Available: https://site.ieee.org/ius-2016/

[81] “Multi-Purpose Multi-Tissue Ultrasound Phantom - CIRS.” Accessed: Mar. 18, 2023. [Online]. Available: https://www.cirsinc.com/products/ultrasound/zerdine-hydrogel/multi-purpose-multi-tisse-ultrasound-phantom/

[82] H. Liebgott, A. Rodriguez-Molares, F. Cervenansky, J. A. Jensen, and O. Bernard, “Plane-wave imaging challenge in medical ultrasound,” in *2016 IEEE International ultrasonics symposium (IUS)*, IEEE, 2016, pp. 1–4.

[83] C. H. Seo, *Improved contrast in ultrasound imaging using dual apodization with cross-correlation*. University of Southern California, 2008.

[84] M. A. Lediju, G. E. Trahey, B. C. Byram, and J. J. Dahl, “Short-lag spatial coherence of backscattered echoes: Imaging characteristics,” *IEEE Trans Ultrason Ferroelectr Freq Control*, vol. 58, no. 7, pp. 1377–1388, 2011.

[85] M. Xu, X. Yang, M. Ding, and M. Yuchi, “Spatio-temporally smoothed coherence factor for ultrasound imaging [correspondence],” *IEEE Trans Ultrason Ferroelectr Freq Control*, vol. 61, no. 1, pp. 182–190, 2014.

[86] "Finding and Using Health Statistics." Accessed: Nov. 26, 2023. [Online]. Available: https://www.nlm.nih.gov/oet/ed/stats/02-900.html

Dealing With Datasets In Hdf5 File Format

Appendix-A:

HDF5 (Hierarchical Data Format version 5) is a data model, library, and file format for storing and managing data. It is designed for flexible and efficient input/output (I/O). It is commonly used in scientific and engineering applications to store large, such as astronomical data, bioimage informatics data, and data from radio telescopes, complex datasets. HDF5 files can store a wide variety of data types, including numerical data, text, images, and more, and it is an open-source file format that is widely used in neuroscience, molecular dynamics, and other fields.

HDF5 files are organized into a hierarchical structure of groups and datasets, which can be easily navigated using the HDF5 library. The format also supports compression and chunking to optimize storage and I/O performance. HDF5 files can be read and written using a variety of programming languages, including MATLAB, Java, Python, and C++.

In MATLAB, the hdf5 library allows users to read and write data to and from HDF5 files. It provides a set of functions and tools that can be used to access and manipulate HDF5 files in MATLAB. With hdf5, users can read and write large datasets, work with complex data structures, and easily exchange data with other software tools that support the HDF5 format.

In MATLAB, the 'hdf5info' function can be used to obtain information about the contents of an HDF5 file. The 'hdf5read' can be used function to read data from an HDF5 file into a MATLAB variable. The 'hdf5write' function used to write data from a MATLAB variable to an HDF5 file. By using the HDF5 file format, large data sets can store and manipulate efficiently, without having to load the entire data set into memory. This can save memory space and reduce the time required to perform data analysis.

To export data from an HDF5 file in MATLAB, the `h5read()` function can be used to read data from the file and then save it to a file in a different format. Here's an example of how to export data from an HDF5 file to a CSV file:

```matlab
% Open the HDF5 file
file = 'example.h5';
h5info(file);

% Read the data from the HDF5 file
data = h5read(file, '/path/to/dataset');

% Save the data to a CSV file
csvwrite('example.csv', data);
```

`h5info()` is used to display information about the HDF5 file, including the names and paths of the datasets it contains. The `h5read()` function is then used to read the data from a specific dataset in the file. Finally, the `csvwrite()` function is used to save the data to a CSV file.

`h5read()` function can also be used to read only a portion of a dataset by specifying a subset of indices. Additionally, the `csvwrite()` function can be replaced with other functions for exporting data to different file formats, such as `save()` for saving data to a MAT file.

There are several advantages of using HDF5 over other file formats like MAT files in MATLAB: first large dataset support: HDF5 can handle significantly larger datasets than MAT files. This is particularly advantageous for scientific data applications where the amount of data can be very large. second Flexibility: HDF5 provides more flexibility in handling data objects in terms of data types and organization. It can store a variety of data types including numerical data, images, audio, and video. third Hierarchical structure: HDF5 has a hierarchical structure that allows for efficient organization of data. This structure of HDF5 files makes it easy to navigate and access data elements. fourth Cross-platform: HDF5 is designed to work on multiple platforms, making it easy to exchange data between different systems. It is also compatible with a variety of programming languages including Python, R, and C++. fifth Compression: HDF5 provides a built-in compression feature that can be used to reduce file size. This can be useful when working with large datasets, as it can reduce storage requirements and improve I/O performance. While HDF5 is a popular open format, it has some drawbacks related to its complex specification, which has initiated discussions for an improved replacement. One alternative to HDF5 is the Experimental Directory Structure (Exdir), which is an open standard for data storage in experimental pipelines. Exdir uses file system directories to represent the hierarchy, with metadata stored in human readable YAML files, datasets stored in binary NumPy files, and raw data stored directly in subdirectories. Storing data in multiple files makes it easier to track for version control.

Publishing

[1] Thanoon, S. A., Alomari, Z., & Al-Zubaidy, M. A. (2023). A New Discrimination Method of Imaging Regions for Improved Ultrafast Ultrasound Imaging Performance. *Journal of Biomedical Photonics & Engineering*, *9*(4), 040310. (Published).

[2] Thanoona, S. A., Alomarib, Z., & Mahmoodb, M. A. Ultrafast ultrasound imaging beamforming techniques: a review. *Muthanna Journal of Engineering and Technology,* Vol. (11), Issue (2), Year (2023). (Published).

المستخلص

يعتبرالتصوير الطبي أداة حديثة تستخدم في تشخيص الأمراض والإصابات، بما في ذلك الأورام والسرطانات. يتم استخدام أنواع مختلفة، بما في ذلك التصوير المقطعي المحوسب والأشعة السينية والتصوير بالرنين المغناطيسي والموجات فوق الصوتية. يحظى التصوير بالموجات فوق الصوتية بشعبية خاصة نظرا لطبيعته غير الجراحية، وفعاليته من حيث التكلفة، وقدرته العالية على تحديد الورم، وعدم الحاجة الى التخدير. مما يوفر معدلات إطارات عالية، ولكنه يضحي بجودة الصورة .يسمى نوع التصوير بالموجات فوق الصوتية الذي لا يستخدم التركيز التصوير بالموجات المستوية (PWI). يعمل الباحثون والمهندسون على تحسين جودة التصوير من خلال تقنيات مختلفة، بما في ذلك تقنيات تشكيل الحزم التكيفية، مع الحد الأدنى من التباين (MV) للشعاع التكيفي الذي يحسن الدقة، والفضاء الذاتي المستند الى حزمة التباين الدنيا (ESBMV)عزز للتباين. ومع ذلك فإن ESBMV له عيب في إنتاج مناطق الصندوق الأسود (BBR) والبقع الداكنة في الصور المنتجة. تم اقتراح طريقة Partial-ESBMV (PESBMV) مؤخرا للتحكم في تلك القطع الأثرية مع انخفاض طفيف في التباين. في هذه الأطروحة، تم اقتراح طريقة تشكيل الحزم لتحسين جودة تصوير الـPESBMV. يستخدم هذا الأسلوب عاملين كأدوات كشف للإشارة بشكل تكيفي إلى المناطق المختلفة للصورة. وهذه العوامل هي عدد المتجهات في مصفوفة الفضاء الفرعي للإشارة التي تنتجها ESBMV ووزن ESBMV. بعد التمييز، الذي يقسم الصورة إلى أربع مناطق، يتم تطبيق أنسب طريقة لتشكيل الحزم في كل منطقة من تلك المناطق. أظهرت نتائج تطبيق الطريقة المقترحة MV و ESBMV و PESBMV على مجموعات البيانات في المختبر وبيانات المحاكاة باستخدام MATLAB (R2021a) تفوق الطريقة المقترحة في تحسين حفظ البقع مع تحسين دقة (55٪) مقارنة بطريقة PESBMV، بالإضافة إلى توفير تباين ممتاز مقارنة بالطرق الأخرى المنفذة.

إقرار لجنة المناقشة

نشهد بأننا أعضاء لجنة التقويم والمناقشة قد اطلعنا على هذه الرسالة الموسومة (**طريقة جديدة لتحسين جودة الصورة في التصوير فوق الصوتي فائق السرعة**) وناقشنا الطالبة (**شهد عبدالسلام ذنون**) في محتوياتها وفيما له علاقة بها بتاريخ / /2024 وقد وجدناها جديرة بنيل شهادة الماجستير/علوم في اختصاص هندسة الاتصالات.

التوقيع:

رئيس اللجنة: أ.م.د. يونس محمود عبوش

التاريخ: /2024/3

التوقيع:

عضو اللجنة: أ.م.د. بسمة محمدكمال يونس

التاريخ: /2024/3

التوقيع:

عضو اللجنة: أ.م.د. صفوان حفيظ يونس

التاريخ:2024/3/١٩

التوقيع:

عضو اللجنة (المشرف): أ.م.د محمود أحمد محمود الزبيدي

التاريخ:2024/3/١٩

التوقيع:

عضو اللجنة (المشرف): م.د زينب رامي العمري

التاريخ:2024/3/١٩

قرار مجلس الكلية

اجتمع مجلس كلية هندسة الالكترونيات بجلسته .... المنعقدة بتاريخ: / / 2024
وقرر المجلس منح الطالبة شهادة الماجستير علوم في اختصاص هندسة الالكترونيك

مقرر المجلس: أ.م.د. بلال علاءالدين جبر

التاريخ: / / 2024

رئيس مجلس الكلية: أ.د. خالد خليل محمد

التاريخ: / /2024

إقرار المشرف

نشهد بأن هذه الرسالة الموسومة (**طريقة جديدة لتحسين جودة الصورة في التصوير فوق الصوتي فائق السرعة**) تم اعدادها من قبل الطالبة (**شهد عبدالسلام ذنون**) تحت اشرافنا في قسم هندسة الاتصالات / كلية هندسة الالكترونيات / جامعة نينوى، وهي جزء من متطلبات نيل شهادة الماجستير/علوم في اختصاص هندسة الاتصالات.

التوقيع:
الاسم: أ.م.د محمود أحمد محمود الزبيدي
التاريخ: 2024/3/19

التوقيع: Z.R Salih
الاسم: م.د. زينب رامي العمري
التاريخ: 2024/3/19

إقرار المقوم اللغوي

اشهد بأنه قد تمت مراجعة هذه الرسالة من الناحية اللغوية وتصحيح ما ورد فيها من أخطاء لغوية وتعبيرية وبذلك أصبحت الرسالة مؤهلة للمناقشة بقدر تعلق الأمر بسلامة الأسلوب أو صحة التعبير.

التوقيع:
الاسم: أ.م.د. **عصام طاهر محمد**
التاريخ: 2024/3/

إقرار رئيس لجنة الدراسات العليا

بناءً على التوصيات المقدمة من قبل المشرف والمقوم اللغوي أرشح هذه الرسالة للمناقشة.

التوقيع:
الاسم: أ.م.د محمود أحمد محمود الزبيدي
التاريخ: 2024/3/19

إقرار رئيس القسم

بناءً على التوصيات المقدمة من قبل المشرف والمقوم اللغوي ورئيس لجنة الدراسات العليا أرشح هذه الرسالة للمناقشة.

التوقيع: 19
الاسم: أ.م.د محمود أحمد محمود الزبيدي
التاريخ: 2024/3/19

وزارة التعليم العالي والبحث العلمي

جامعة نينوى

كلية هندسة الالكترونيات

قسم هندسة الاتصالات

طريقة جديدة لتحسين جودة الصورة في التصوير فوق الصوتي فائق السرعة

رسالة تقدمت بها

شهد عبد السلام ذنون

إلى

مجلس كلية هندسة الالكترونيات

جامعة نينوى

كجزء من متطلبات نيل شهادة الماجستير

في

هندسة الاتصالات

باشراف

أ.م.د. محمود أحمد محمود الزبيدي

د. زينب رامي صالح العُمري

١٤٤٥ هـ **٢٠٢٤م**

وزارة التعليم العالي والبحث العلمي
جامعة نينوى
كلية هندسة الالكترونيات
قسم هندسة الاتصالات

طريقة جديدة لتحسين جودة الصورة في التصوير فوق الصوتي فائق السرعة

شهد عبد السلام ذنون

رسالة ماجستير علوم في هندسة الاتصالات

باشراف

أ.م.د. محمود أحمد محمود الزبيدي

د.زينب رامي صالح العُمري

١٤٤٥هـ ٢٠٢٤م